

Stellar laboratories

VI. New Mo^{IV} – VII oscillator strengths and the molybdenum abundance in the hot white dwarfs G191–B2B and RE 0503–289*

T. Rauch¹, P. Quinet^{2,3}, D. Hoyer¹, K. Werner¹, M. Demleitner⁴, and J. W. Kruck⁵

¹ Institute for Astronomy and Astrophysics, Kepler Center for Astro and Particle Physics, Eberhard Karls University, Sand 1, 72076 Tübingen, Germany
e-mail: rauch@astro.uni-tuebingen.de

² Physique Atomique et Astrophysique, Université de Mons – UMONS, 7000 Mons, Belgium

³ IPNAS, Université de Liège, Sart Tilman, 4000 Liège, Belgium

⁴ Astronomisches Rechen-Institut, Zentrum für Astronomie, Ruprecht Karls University, Mönchhofstraße 12–14, 69120 Heidelberg, Germany

⁵ NASA Goddard Space Flight Center, Greenbelt, MD 20771, USA

Received 8 September 2015; accepted 15 December 2015

ABSTRACT

Context. For the spectral analysis of high-resolution and high signal-to-noise (S/N) spectra of hot stars, state-of-the-art non-local thermodynamic equilibrium (NLTE) model atmospheres are mandatory. These are strongly dependent on the reliability of the atomic data that is used for their calculation.

Aims. To identify molybdenum lines in the ultraviolet (UV) spectra of the DA-type white dwarf G191–B2B and the DO-type white dwarf RE 0503–289 and, to determine their photospheric Mo abundances, reliable Mo^{IV}–VII oscillator strengths are used.

Methods. We newly calculated Mo^{IV}–VII oscillator strengths to consider their radiative and collisional bound-bound transitions in detail in our NLTE stellar-atmosphere models for the analysis of Mo lines exhibited in high-resolution and high S/N UV observations of RE 0503–289.

Results. We identified 12 Mo^V and nine Mo^{VI} lines in the UV spectrum of RE 0503–289 and measured a photospheric Mo abundance of $1.2 - 3.0 \times 10^{-4}$ (mass fraction, 22 500 – 56 400 times the solar abundance). In addition, from the As^V and Sn^{IV} resonance lines, we measured mass fractions of arsenic ($0.5 - 1.3 \times 10^{-5}$, about 300 – 1200 times solar) and tin ($1.3 - 3.2 \times 10^{-4}$, about 14 300 – 35 200 times solar). For G191–B2B, upper limits were determined for the abundances of Mo (5.3×10^{-7} , 100 times solar) and, in addition, for Kr (1.1×10^{-6} , 10 times solar) and Xe (1.7×10^{-7} , 10 times solar). The arsenic abundance was determined ($2.3 - 5.9 \times 10^{-7}$, about 21 – 53 times solar). A new, registered German Astrophysical Virtual Observatory (GAVO) service, TOSS, has been constructed to provide weighted oscillator strengths and transition probabilities.

Conclusions. Reliable measurements and calculations of atomic data are a prerequisite for stellar-atmosphere modeling. Observed Mo^V–VI line profiles in the UV spectrum of the white dwarf RE 0503–289 were well reproduced with our newly calculated oscillator strengths. For the first time, this allowed the photospheric Mo abundance in a white dwarf to be determined.

Key words. atomic data – line: identification – stars: abundances – stars: individual: G191–B2B – stars: individual: RE 0503–289 – virtual observatory tools

1. Introduction

RE 0503–289 (WD 0501–289, McCook & Sion 1999a,b) is a hot, helium-rich, DO-type white dwarf (WD, effective temperature $T_{\text{eff}} = 70\,000$ K, surface gravity $\log(g/\text{cm/s}^2) = 7.5$, Dreizler & Werner 1996), that exhibits lines of at least ten trans-iron elements in its far-ultraviolet (FUV) spectrum (Werner et al. 2012b). The abundance analysis of these species is hampered by the lack of atomic data for their higher ionization stages, i.e.,

* Based on observations with the NASA/ESA Hubble Space Telescope, obtained at the Space Telescope Science Institute, which is operated by the Association of Universities for Research in Astronomy, Inc., under NASA contract NAS5-26666.

** Based on observations made with the NASA-CNES-CSA Far Ultraviolet Spectroscopic Explorer.

*** Tables 11 to 14 are only available via the German Astrophysical Virtual Observatory (GAVO) service TOSS (<http://dc.g-vo.org/TOSS>).

IV–VII. While Werner et al. (2012b) could measure only the Kr and Xe abundances, further abundance determinations (Zn, Ge, Ga, Xe, and Ba by Rauch et al. 2014a, 2012, 2014b, 2015b,a, respectively) were always initiated by new calculations of reliable transition probabilities.

G191–B2B (WD 0501+527, McCook & Sion 1999a,b) is a hot, hydrogen-rich, DA-type white dwarf that was recently analyzed by Rauch et al. (2013, $T_{\text{eff}} = 60\,000$ K, $\log g = 7.6$). Based on this model, Rauch et al. (2014a,b, 2015b) measured the abundances of Zn, Ba, and Ga.

Molybdenum is another trans-iron element (atomic number $Z = 42$). It was discovered for the first time in a WD (in the spectrum of RE 0503–289) by Werner et al. (2012b, four Mo^{VI} lines). To identify more lines of Mo and to determine its abundance, we calculated new transition probabilities for Mo^{IV}–VII.

In this paper, we first describe the available observations (Sect. 2), our stellar-atmosphere models (Sect. 3), and the com-

putation of the new transition probabilities (Sect. 4). A new Virtual Observatory (VO) service that provides access to transition probabilities is presented in Sect. 5.

To use the most elaborated models of G191–B2B and RE 0503–289 for our Mo abundance analysis, we start with an incorporation and an abundance determination of arsenic (Sect. 6.1, both stars) and tin (Sect. 6.2, RE 0503–289). Then, we assess the Mo photospheric abundances in RE 0503–289 and G191–B2B (Sect. 6.3). In Sect. 6.5, we determine upper abundance limits of krypton and xenon in G191–B2B. To understand the abundance patterns of trans-iron elements, we investigate on the efficiency of radiative levitation acting on the elements Zn, Ga, Ge, As, Kr, Mo, Sn, Xe, and Ba in both stars' atmospheres (Sect. 7). We summarize our results and conclude in Sect. 8.

2. Observations

G191–B2B We used the spectra obtained with the Far Ultraviolet Spectroscopic Explorer (FUSE, $910 \text{ \AA} < \lambda < 1190 \text{ \AA}$, resolving power $R = \lambda/\Delta\lambda \approx 20\,000$, for details see Rauch et al. 2013) and the Hubble Space Telescope / Space Telescope Imaging Spectrograph (HST/STIS, $1145 \text{ \AA} < \lambda < 3145 \text{ \AA}$, resolution of $\approx 3 \text{ km/s}$, see Rauch et al. 2013, available at <http://www.stsci.edu/hst/observatory/cdbs/calspec.html>).

RE 0503–289 We analyzed its FUSE (described in detail by Werner et al. 2012b) and HST/STIS observations ($1144 \text{ \AA} < \lambda < 3073 \text{ \AA}$). The latter was co-added from two observations with grating E140M (exposure times 2493 s and 3001 s, $1144 \text{ \AA} - 1709 \text{ \AA}$, $R \approx 45\,800$), and two observations with grating E230M (1338 s, $1690 \text{ \AA} - 2366 \text{ \AA}$ and 1338 s, $2277 \text{ \AA} - 3073 \text{ \AA}$, $R \approx 30\,000$). These STIS observations are retrievable from the Barbara A. Mikulski Archive for Space Telescopes (MAST).

3. Model atmospheres and atomic data

We employed the Tübingen NLTE¹ Model Atmosphere Package (TMAP², Werner et al. 2003, 2012a) to calculate plane-parallel, chemically homogeneous model-atmospheres in hydrostatic and radiative equilibrium. Model atoms were taken from the Tübingen Model Atom Database (TMAD³, Rauch & Deetjen 2003) that has been constructed as part of the Tübingen contribution to the German Astrophysical Virtual Observatory (GAVO⁴). For our Mo model atoms, we follow Rauch et al. (2015b) and used a statistical approach to calculate so-called super levels and super lines with our Iron Opacity and Interface (IrOnIc⁵, Rauch & Deetjen 2003). We transferred our new Mo data into Kurucz-formatted files⁶ that were then ingested and processed by IrOnIc. The statistics of our Mo model atom is summarized in Table 1.

For Mo and all other species, level dissolution (pressure ionization) following Hummer & Mihalas (1988) and Hubeny et al. (1994) is accounted for. Broadening for all Mo lines that are due to the quadratic Stark effect is calculated using approximate formulae by Cowley (1970, 1971).

Table 1. Statistics of Mo IV – VII atomic levels and line transitions from Tables 11 – 14, respectively.

ion	Atomic levels	Lines	Super levels	Super lines
IV	162	2803	7	15
V	257	5882	7	22
VI	112	988	7	23
VII	95	1181	7	16
	626	10824	28	76

4. Atomic structure and radiative data calculation

New calculations of oscillator strengths for a large number of transitions of molybdenum ions that are considered in the present work were carried out using the pseudo-relativistic Hartree-Fock (HFR) method (Cowan 1981), including core-polarization corrections (see, e.g., Quinet et al. 1999, 2002).

For Mo IV, the configuration interaction was considered among the configurations $4d^3$, $4d^25s$, $4d^26s$, $4d^25d$, $4d^26d$, $4d4f^2$, $4d5s^2$, $4d5p^2$, $4d5d^2$, $4d5s5d$, $4d5p4f$, $4d5p5f$, and $4d4f5f$ for the even parity and $4d^25p$, $4d^26p$, $4d^24f$, $4d^25f$, $4d5s5p$, $4d5s4f$, $4d5s5f$, $4d5p5d$, $4d4f5d$, and $4d5d5f$ for the odd parity. The core-polarization parameters were the dipole polarizability of a Mo VII ionic core reported by Fraga et al. (1976), i.e., $\alpha_d = 1.82 \text{ a.u.}$, and the cut-off radius corresponding to the HFR mean value $\langle r \rangle$ of the outermost core orbital (4p), i.e., $r_c = 1.20 \text{ a.u.}$ Using the experimental energy levels reported by Sugar & Musgrove (1988) and Cabeza et al. (1989), the radial integrals (average energy, Slater, spin-orbit and effective interaction parameters) of $4d^3$, $4d^25s$, $4d^26s$, $4d^25d$, and $4d^25p$ configurations were adjusted by a well-established least-squares fitting process that minimizes the differences between computed and experimental energies.

For Mo V, the configurations retained in the HFR model were $4d^2$, $4d5s$, $4d6s$, $4d5d$, $4d6d$, $4d5g$, $5s^2$, $5p^2$, $5d^2$, $4f^2$, $5s5d$, $5s6s$, $5p4f$, $5p5f$, $4p^54d^24f$, $4p^54d^25f$, and $4p^54d^25p$ for the even parity and $4d5p$, $4d6p$, $4d4f$, $4d5f$, $4d6f$, $4d7f$, $4d8f$, $4d9f$, $5s5p$, $5p5d$, $5s4f$, $5s5f$, $4f5d$, $4p^54d^3$, $4p^54d^25s$, and $4p^54d^25d$ for the odd parity. In this ion, the semi-empirical process was performed to optimize the radial integrals corresponding to $4d^2$, $4d5s$, $4d6s$, $4d5d$, $4d5g$, $5s^2$, $5p^2$, $5s5d$, $5s6s$, $4d5p$, $4d6p$, $4d4f$, $4d5f$, $4d6f$, $4d7f$, $4d8f$, $4d9f$, $5s5p$, $5s4f$, and $4p^54d^3$ configurations, which use the experimental energy levels reported by Reader & Tauheed (2015). Core-polarization effects were estimated using a dipole polarizability value corresponding to a Mo VIII ionic core taken from Fraga et al. (1976), i.e., $\alpha_d = 1.48 \text{ a.u.}$, and a cut-off radius equal to 1.20 a.u.

In the case of Mo VI, the $4d$, $5d$, $6d$, $7d$, $8d$, $5s$, $6s$, $7s$, $8s$, $5g$, $6g$, $7g$, $8g$, $7i$, $8i$, $4p^54d5p$, $4p^54d4f$, and $4p^54d5f$ even configurations and the $5p$, $6p$, $7p$, $8p$, $9p$, $10p$, $11p$, $4f$, $5f$, $6f$, $7f$, $8f$, $9f$, $6h$, $7h$, $8h$, $8k$, $4p^54d^2$, $4p^54d5s$, and $4p^54d5d$ odd configurations were explicitly included in the HFR model with the same core-polarization parameters as those considered for Mo V. The semi-empirical optimization process was carried out to fit the radial parameters in the nd ($n = 4 – 8$), ns ($n = 5 – 8$), ng ($n = 5 – 8$), ni ($n = 7 – 8$), np ($n = 5 – 11$), nf ($n = 4 – 9$), nh ($n = 6 – 8$), $8k$, $4p^54d^2$, and $4p^54d5s$ configurations using the experimental energy levels published by Reader (2010).

Finally, for Mo VII, the HFR multiconfiguration expansions included the $4p^6$, $4p^55p$, $4p^56p$, $4p^54f$, $4p^55f$, $4p^56f$, $4s4p^64d$, $4s4p^65d$, $4s4p^66d$, $4s4p^65s$, $4s4p^66s$, $4p^44d^2$, $4p^44d5s$, and $4p^45s^2$ even configurations and the $4p^54d$, $4p^55d$, $4p^56d$, $4p^55s$, $4p^56s$, $4p^57s$, $4p^58s$, $4p^59s$, $4p^510s$, $4p^55g$, $4p^56g$, $4s4p^65p$,

¹ non-local thermodynamic equilibrium

² <http://astro.uni-tuebingen.de/~TMAP>

³ <http://astro.uni-tuebingen.de/~TMAD>

⁴ <http://www.g-vo.org>

⁵ <http://astro.uni-tuebingen.de/~TIRO>

⁶ GFxxxy.GAM, GFxxxy.LIN, and GFxxxy.POS files with xx = element number, yy = element charge, <http://kurucz.harvard.edu/atoms.html>

$4s4p^66p$, $4s4p^64f$, $4s4p^65f$, $4s4p^66f$, $4p^44d5p$, and $4p^44d4f$ odd configurations. Here, because some configurations with open 4s and 4p orbitals were explicitly included in the physical model, the core-polarization effects were estimated by considering a Mo XV ionic core with the corresponding dipole polarizability value taken from Johnson et al. (1983), i.e., $\alpha_d = 0.058$ a.u., and a cut-off radius equal to 0.41 a.u., which corresponds to the HFR mean value $\langle r \rangle$ of the 3d subshell. The fitting process was then carried out with the experimental energy levels classified by Sugar & Musgrove (1988) and Shirai et al. (2000) to adjust the radial parameters that characterize the $4p^6$, $4p^55p$, $4p^54f$, $4p^55f$, $4s4p^64d$, $4p^44d^2$, $4p^54d$, $4p^55d$, $4p^5ns$ ($n = 5 - 10$), $4p^55g$, and $4s4p^65p$ configurations. The parameters adopted in our computations are summarized in Tables 2 - 5 and computed and available experimental energies are compared in Tables 6 - 9, for Mo IV-VII, respectively.

Tables 11 - 14 give the weighted HFR oscillator strengths ($\log gf$) and transition probabilities (gA , in s^{-1}) for Mo IV-VII, respectively, and the numerical values (in cm^{-1}) of lower and upper energy levels and the corresponding wavelengths (in Å). In the last column of each table, we also give the absolute value of the cancellation factor CF, as defined by Cowan (1981). We note that very low values of this factor (typically < 0.05) indicate strong cancellation effects in the calculation of line strengths. In these cases, the corresponding gf and gA values could be very inaccurate and, therefore, need to be considered with some care. However, very few of the transitions that appear in Tables 11 - 14 are affected. These tables are provided via the newly developed GAVO Tübingen Oscillator Strengths Service TOSS⁷ that is briefly described in Sect. 5.

Oscillator strengths were published by Reader & Tauheed (2015) for 923 lines of Mo V and by Reader (2010) for 245 lines of Mo VI. We compared $\log gf$ values and wavelengths of those lines whose positions agree with those of our lines within $\Delta\lambda \leq 0.02$ Å (these are 921 lines of Mo V, 178 lines of Mo VI) (Figs. 1 and 2). In general, we find a rather good agreement, although our new $\log gf$ -values seem to be, on average, smaller than those previously published. This can be explained by the fact that our calculations explicitly include a larger set of interacting configurations, in particular with an open 4p subshell, as well as a pseudo-potential modeling of the remaining core-valence electronic correlations. For the Mo V and Mo VI lines that were identified in RE 0503–289 (Table 10, Fig. 12) and were used for the abundance determination, the $\log gf$ -values are almost identical.

5. The GAVO service TOSS

In the framework of the GAVO project, we developed the new, registered VO service TOSS. It is designed to provide easy access to calculated oscillator strengths and transition probabilities of any kind in VO-compliant format.

Line data is stored in terms of the Spectral Line Data Model (Osuna et al. 2010) and is accessible through a web browser interface, via the Simple Line Access Protocol SLAP (Salgado et al. 2010), and via the Table Access Protocol TAP (Dowler et al. 2010). The browser-based interface offers a web form, which allows conventional queries by wavelength, element, ion-

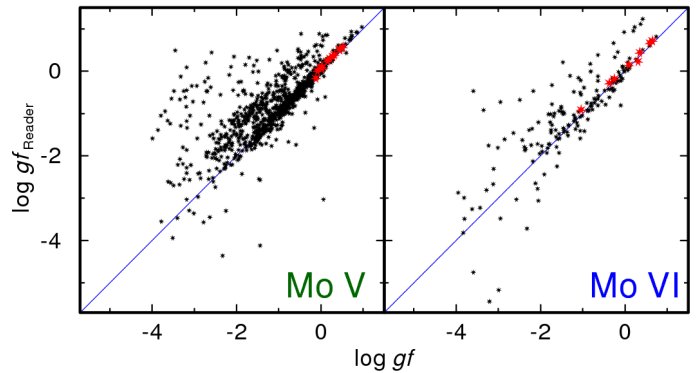


Fig. 1. Comparison of our weighted oscillator strengths to those of Reader & Tauheed (2015) for Mo V (left panel) and of Reader (2010) for Mo VI (right). The larger, red symbols refer to the lines identified in RE 0503–289 (Table 10).

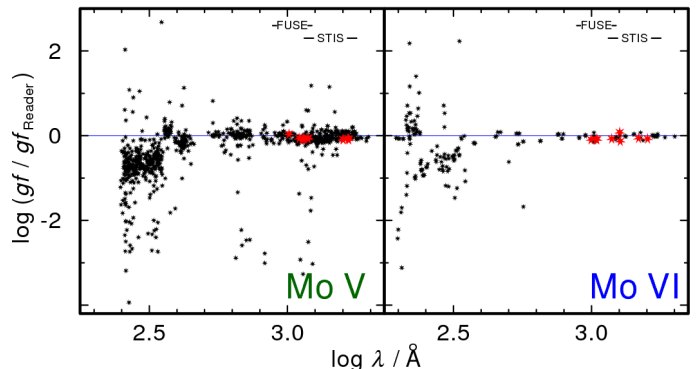


Fig. 2. Ratio of our weighted oscillator strengths and those of Reader & Tauheed (2015) for Mo V (left panel) and of Reader (2010) for Mo VI (right). The wavelength ranges of our FUSE and HST/STIS spectra are marked. The larger, red symbols refer to the lines identified in RE 0503–289 (Table 10).

isation stage, etc., exporting to various tabular formats and also directly into user programs via SAMP⁸.

The SLAP interface can be used from specialized programs (“SLAP clients”) like VOSpec (Osuna et al. 2005); this is normally transparent to the user; in a server selector, the service will typically appear under its short name TOSS SLAP.

The TAP interface allows database queries against the line database, including comparisons with user-provided data (“uploads”). In the TAP dialogs of applications like TOPCAT, the user should look for “GAVO DC” or manually enter the access URL <http://dc.g-vo.org/tap>. As the discussion of TAP’s possibilities is beyond the scope of this paper, see on-line examples for TOSS service usage⁹.

6. Photospheric abundances

To improve the simulation of the background opacity, we included As in our calculations for G191–B2B and RE 0503–289 and determined its abundance from these models (Sect. 6.1). Then, we included Sn for RE 0503–289 (Sect. 6.2) because our new HST/STIS observation provides access to Sn IV lines that are necessary for an abundance analysis. Based on these extended

⁸ The Simple Application Messaging Protocol is a VO-defined standard protocol facilitating seamless and fast data exchange on user desktops.

⁹ <http://dc.g-vo.org/toss/q/q/examples>

⁷ <http://dc.g-vo.org/TOSS>

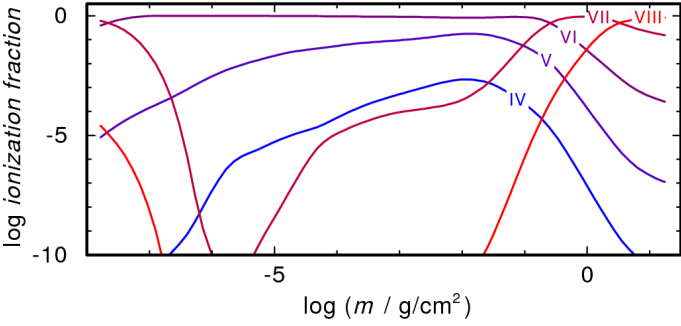


Fig. 3. Arsenic ionization fractions in our RE 0503–289 model. m is the column mass, measured from the outer boundary of the model atmosphere.

models, we considered Mo and determined its abundances for RE 0503–289 (Sect. 6.3) and G191–B2B (Sect. 6.4).

6.1. G191–B2B and RE 0503–289: Arsenic ($Z = 33$)

In the FUSE observation of RE 0503–289, Werner et al. (2012b) discovered As v $\lambda\lambda 987.65, 1029.48, 1051.6, 1056.7 \text{ \AA}$. For As v, lifetimes were measured with the beam-foil technique (Pinnington et al. 1981). The multiplet f-value (0.78 ± 0.06) of the As v resonance transition was determined with the help of arbitrarily normalized decay curve (ANDC) analyses, which were confirmed by calculations of Fischer (1977), Migdalek & Baylis (1979), and Curtis & Theodosiou (1989). Morton (2000) lists both components in his compilation, $\lambda 987.65 \text{ \AA}$ ($4s^2 S_{1/2} - 4p^2 P_{3/2}^0$, $f = 0.528$) and $\lambda 1029.48 \text{ \AA}$ ($4s^2 S_{1/2} - 4p^2 P_{1/2}^0$, $f = 0.253$). These were used by Chayer et al. (2015) to determine arsenic mass fractions. They found 6.3×10^{-8} (6 times solar) and 1.6×10^{-5} (1450 times solar) in G191–B2B and RE 0503–289, respectively.

As v $\lambda\lambda 1051.6, 1056.7 \text{ \AA}$ belong to the $4d^2 D - 4f^2 F^o$ multiplet ($\lambda\lambda 1050.67, 1051.64, 1055.60, 1056.58$) but no oscillator strengths have been calculated so far.

We included the TMAD As iv-viii model atom in our model-atmosphere calculations. As vi is the dominant ion in the line-forming region in both stars (Figs. 3 and 4). We reproduced the observed As v $\lambda\lambda 987.65, 1029.48 \text{ \AA}$ line profiles well in the FUSE spectra of G191–B2B and RE 0503–289 at mass fractions of 3.7×10^{-7} (29 times solar) and 8.3×10^{-6} (760 times solar), respectively (Fig. 5). Our abundances deviate by factors of 6 and 0.5 for G191–B2B and RE 0503–289, respectively, from those of Chayer et al. (2015), who made an LTE assumption because of lack of atomic data. Both stars are out of the validity domain for LTE modeling (e.g., Rauch 2012), which is corroborated by an inspection of the departure coefficients (ratio of NLTE to LTE occupation numbers) of the five lowest As v levels in our models for G191–B2B and RE 0503–289 that deviate from unity (Fig. 6 and 7, respectively). Therefore, the results of an LTE analysis may be afflicted by a large systematic error.

Figure 8 shows a comparison of theoretical profiles of As v $\lambda\lambda 987.65, 1029.48 \text{ \AA}$ that are calculated from our NLTE model and an LTE model (calculated by TMAD based on the temperature and density stratification of the NLTE model, LTE occupation numbers of the atomic levels are enforced by an artificial increase of all collisional rates by a factor of 10^{20}). In the case of G191–B2B, the LTE profiles are too strong and, thus, the abundance had to be reduced to 1.0×10^{-7} to match the observation. For RE 0503–289, they are too weak and, thus, a higher

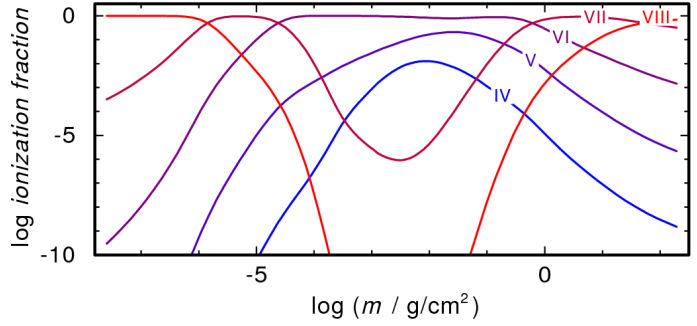


Fig. 4. As in Fig. 3, for G191–B2B.

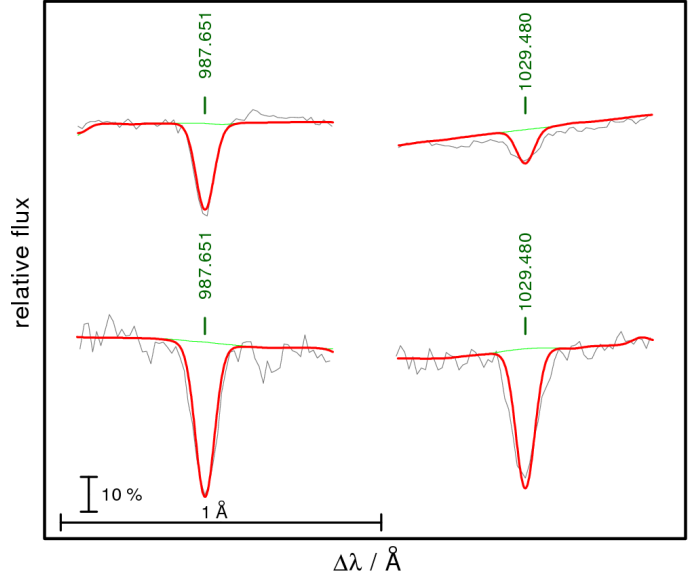


Fig. 5. Sections of our FUSE observations of G191–B2B (top row) and RE 0503–289 (bottom row) around As v $\lambda 987.65 \text{ \AA}$ (left column) and As v $\lambda 1029.48 \text{ \AA}$ (right column). The thick red and thin green lines show a comparison with theoretical spectra of two models, with and without As, respectively.

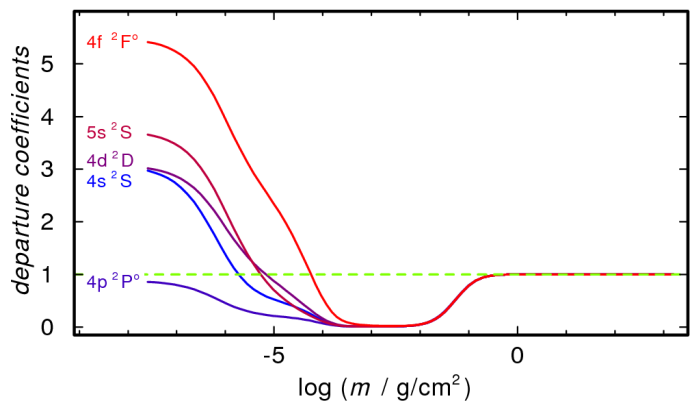


Fig. 6. Departure coefficients of the five lowest As v levels in the model for G191–B2B.

abundance of 1.7×10^{-5} is needed to reproduce the observation. This may explain, in part, the deviation of our As abundances from those of Chayer et al. (2015).

However, a precise abundance analysis by means of NLTE model-atmosphere techniques requires reliable oscillator strengths, not only for the lines employed in the abundance determination, but for the complete model atom that is considered

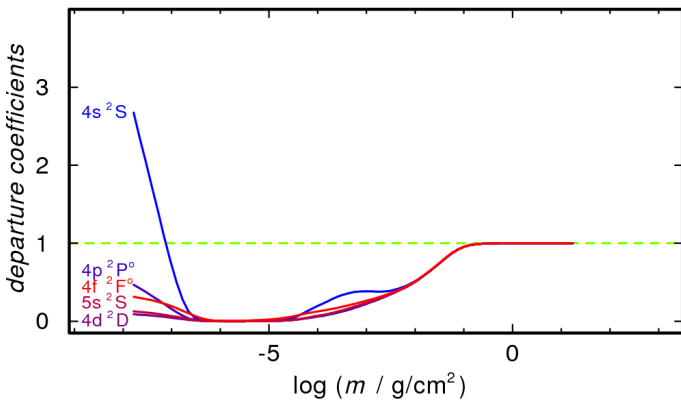


Fig. 7. As for Fig. 6, for RE 0503–289.

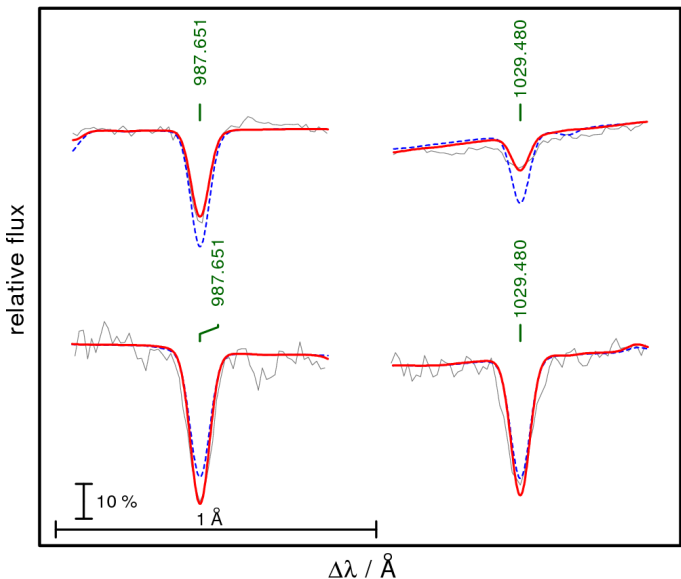


Fig. 8. As for Fig. 5, the thick red and dashed blue lines show a comparison with theoretical spectra of NLTE and LTE models, respectively.

in the model-atmosphere and spectral-energy-distribution calculations. Once these oscillator strengths become available for a large number of As v–vii lines, it will be possible to construct much more complete As model ions and a new determination of the As abundance will be more precise.

6.2. RE 0503–289: Tin ($Z = 50$)

Rauch et al. (2013) measured the Sn abundance in G191–B2B (3.53×10^{-7} , 37 times solar). They used the lines of the resonance doublet, namely, Sn iv $\lambda 1314.537 \text{ Å}$ ($5s^2S_{1/2} - 5p^2P_{3/2}$, $f = 0.637$) and $\lambda 1437.525 \text{ Å}$ ($5s^2S_{1/2} - 5p^2P_{1/2}$, $f = 0.240$). Their f-values were calculated by Morton (2000) based on energy levels provided by Moore (1958). These lines are visible in our HST/STIS spectrum of RE 0503–289 as well. To determine the Sn abundance, we used the same model atom like Rauch et al. (2013) and reproduced the observed line profiles of both lines (Fig. 9) well at a mass fraction of 2.04×10^{-4} (about 22 500 times solar). This Sn abundance analysis will also be improved, as soon as reliable transition probabilities for Sn iv–vi are published.

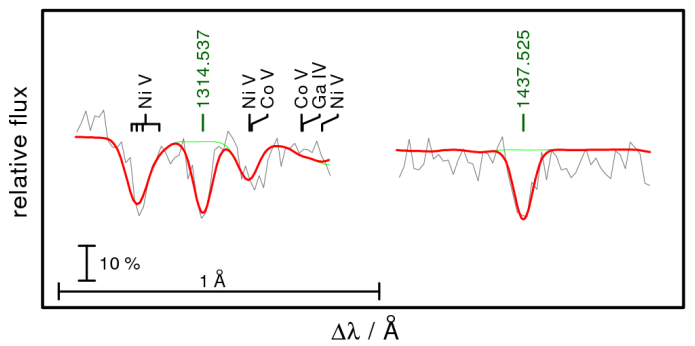


Fig. 9. Sections of our HST/STIS observations of RE 0503–289 around Sn iv $\lambda 1314.537 \text{ Å}$ (left) and Sn iv $\lambda 1437.525 \text{ Å}$ (right). The thick, red and thin, green lines show a comparison with theoretical spectra of two models with and without Sn, respectively.

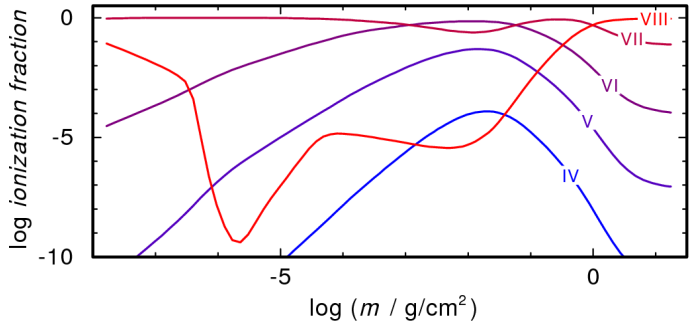


Fig. 10. Molybdenum ionization fractions in our RE 0503–289 model.

6.3. RE 0503–289: Molybdenum

Our RE 0503–289 model ($T_{\text{eff}} = 70\,000 \text{ K}$, $\log g = 7.5$) includes opacities of H, He, C, N, O, Si, P, S, Ca, Sc, Ti, V, Cr, Mn, Fe, Co, Ni, Zn, Ga, Ge, As, Kr, Mo, Xe, and Ba. Figure 10 shows the Mo ionization fractions in this model. Mo vi+vii are the dominating ionization stages in the line-forming region ($-4.0 \lesssim \log m \lesssim 0.5$). The element abundances are given in Table 15. In general, their uncertainty is about 0.2 dex. This includes the error propagation due to the error ranges of T_{eff} (cf., e.g., Vennes & Lanz 2001), $\log g$, and the background opacity.

Figure 11 shows the relative line strengths (normalized to that of Mo vi $\lambda 1038.642 \text{ Å}$) of the Mo lines in the synthetic spectrum of RE 0503–289. We note that these strengths reduce if the spectrum is convolved with a Gaussian to match the instruments’ resolutions (Sect. 2).

In the FUSE and HST/STIS observations, we identified 12 Mo v and nine Mo vi lines (Fig. 12). Their strengths were well reproduced at a Mo abundance of 1.88×10^{-4} (mass fraction), which is 35 400 times the solar value (Grevesse et al. 2015). Many more weak Mo v and Mo vi lines are visible in the synthetic spectrum but they fade in the noise of the presently available observations. The search for the strongest Mo iv and Mo vii lines (Fig. 11) was not successful. This was not unexpected, given the predicted weakness of the lines and the S/N of the data. Figure 13 shows the two strongest Mo vii lines of our model. We note that Ba vii $\lambda 1255.520 \text{ Å}$ dominates the observed absorption around $\lambda 1255.5 \text{ Å}$ (Fig. 13).

The identification of Mo lines in the wavelength region $\lambda \gtrsim 1700 \text{ Å}$ was strongly hampered by the lower signal-to-noise (S/N) and resolution (only a fourth of the exposure time and 66 % of the resolving power of the spectrum, compared to the region at $\lambda \lesssim 1700 \text{ Å}$, see Sect. 2). An example is shown in

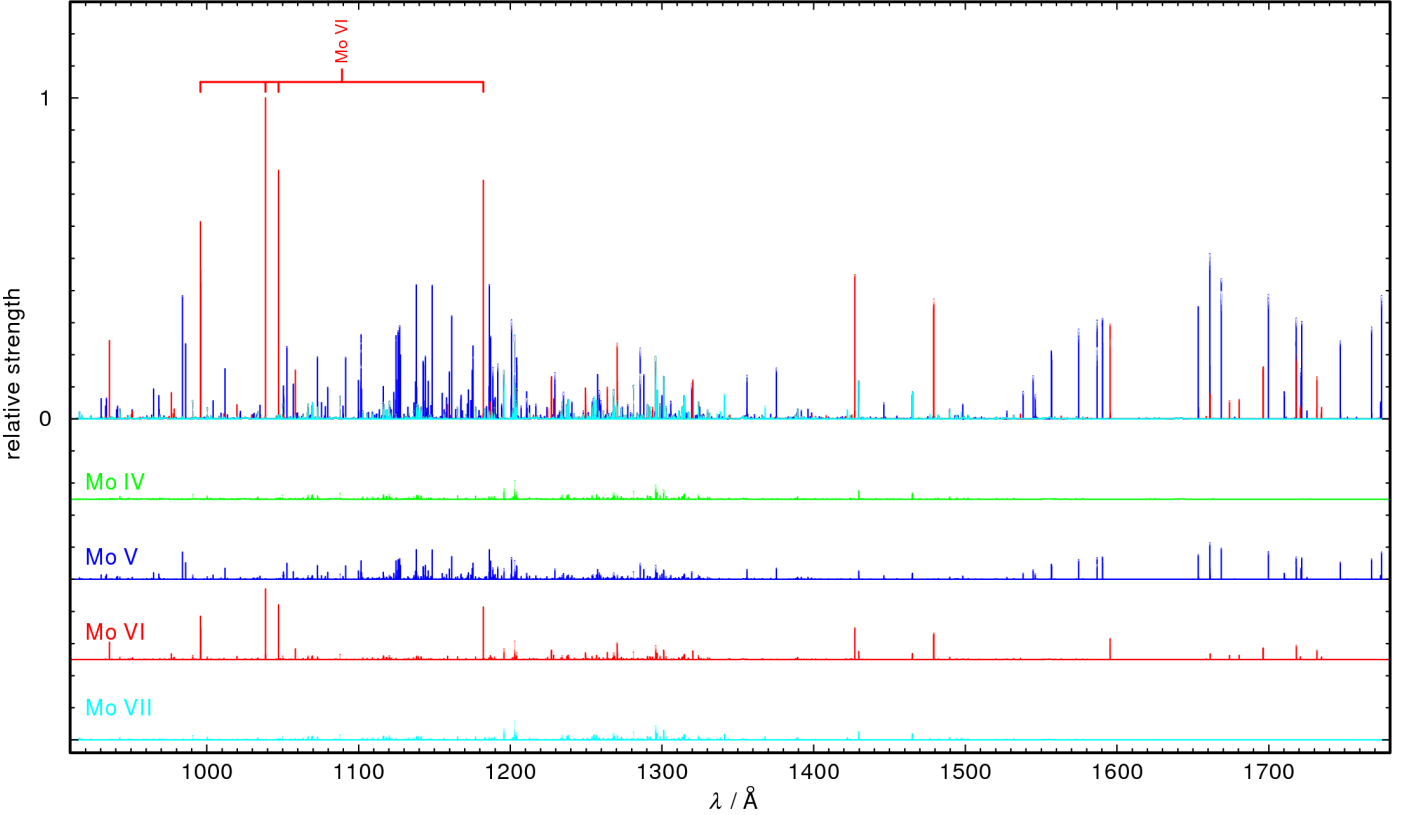


Fig. 11. Relative strengths of Mo lines calculated from our stellar-atmosphere model of RE 0503–289. Top panel: Mo_{IV}–VII lines, the four most prominent are Mo_{VI} lines that were identified by Werner et al. (2012b) are marked. Graphs 2 to 5 (from top to bottom): lines of individual Mo_{IV}–VII ions (intensities reduced by a factor of 0.22 compared to the top panel), respectively.

Table 15. Photospheric abundances of RE 0503–289. IG is a generic model atom (Rauch & Deetjen 2003) comprising Ca, Sc, Ti, V, Cr, Mn, and Co. [X] denotes log (fraction / solar fraction) of species X.

Element	Mass	Number	[X]
	Fraction		
He	9.74×10^{-1}	9.92×10^{-1}	0.592
C	2.23×10^{-2}	7.56×10^{-3}	0.974
N	1.73×10^{-4}	5.04×10^{-5}	-0.602
O	1.97×10^{-3}	5.01×10^{-4}	-0.464
Si	1.61×10^{-4}	2.33×10^{-5}	-0.617
P	1.15×10^{-6}	1.51×10^{-7}	-0.705
S	3.96×10^{-5}	5.04×10^{-6}	-0.892
IG	1.00×10^{-6}	9.19×10^{-8}	-1.787
Fe	$< 1.30 \times 10^{-5}$	$< 9.50 \times 10^{-7}$	< -1.967
Ni	7.26×10^{-5}	5.04×10^{-6}	0.028
Zn	1.13×10^{-4}	7.05×10^{-6}	1.814
Ga	3.45×10^{-5}	2.02×10^{-6}	2.810
Ge	1.59×10^{-4}	8.90×10^{-6}	2.845
As	8.27×10^{-6}	4.50×10^{-7}	2.879
Kr	5.05×10^{-5}	2.46×10^{-6}	2.666
Mo	1.88×10^{-4}	8.00×10^{-6}	4.549
Sn	2.04×10^{-4}	7.00×10^{-6}	4.351
Xe	6.30×10^{-5}	1.96×10^{-6}	3.577
Ba	3.58×10^{-4}	1.06×10^{-5}	4.301

Fig. 14. Mo_V $\lambda 1718.088 \text{ \AA}$ appears at comparable strengths of other lines that were identified (Fig. 12). However, it is within

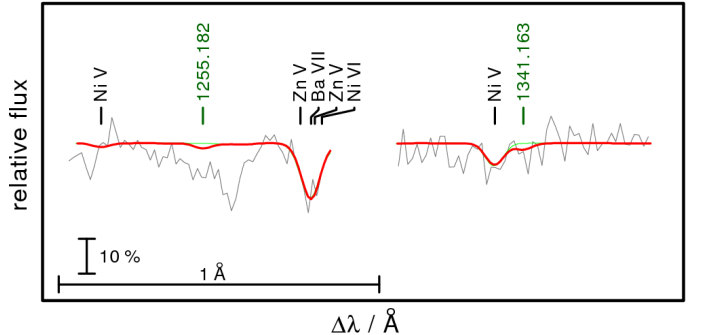


Fig. 13. Same as Fig. 12, for two Mo_{VII} lines.

the noise level of the observation and has to be judged uncertain. Mo_{VI} $\lambda 1718.238 \text{ \AA}$ is weaker but a better observation would allow an identification.

6.4. G191–B2B: Molybdenum

We added Mo into our atmosphere model ($T_{\text{eff}} = 60\,000 \text{ K}$, $\log g = 7.6$) for G191–B2B, which considers H, He, C, N, O, Al, Si, P, S, Ca, Sc, Ti, V, Cr, Mn, Fe, Co, Ni, Zn, Ga, Ge, As, Mo, Sn, and Ba. The abundances are given in Table 16. Mo_{VI}+VII are the dominating ionization fractions in the line-forming region (Fig. 15).

We performed a search for Mo lines in the observed spectra of G191–B2B, analogous to that in Sect. 6.3. However, we did not identify any. Figure 16 shows a comparison of our synthetic spectra to the observations. Since the HST/STIS spectrum of

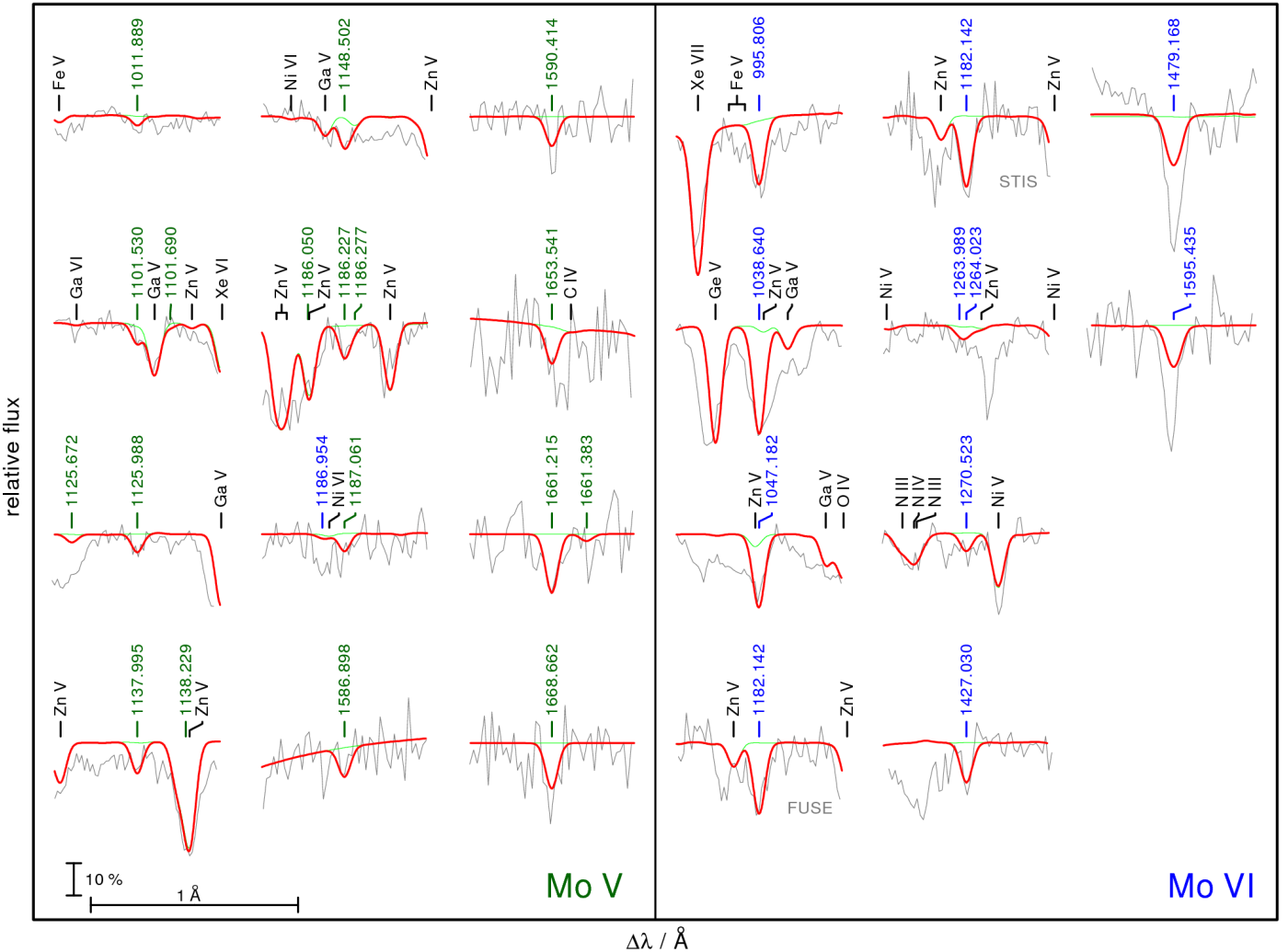


Fig. 12. Mo^V lines (left panel, marked with their wavelengths from Table 12 in Å, green in the online version) and Mo^{VI} lines (right panel, marked blue, wavelengths from Table 13) in the FUSE (for lines at $\lambda < 1188 \text{ \AA}$) and HST/STIS ($\lambda > 1188 \text{ \AA}$) observations of RE 0503–289. The synthetic spectra are convolved with a Gaussian (full width at half maximum = FWHM = 0.06 Å) to simulate the instruments' resolutions. Other identified photospheric lines are marked in black. The thick red and thin green lines show a comparison with theoretical spectra of two models with and without Mo, respectively. The vertical bar indicates 10 % of the continuum flux.

G191–B2B (Sect. 2) is of excellent quality, Mo^{VI} $\lambda 1469.168 \text{ \AA}$ gives a stringent upper abundance limit of 5.3×10^{-7} by mass (about 100 times solar, Grevesse et al. 2015).

6.5. G191–B2B: Krypton (Z = 36) and Xenon (Z = 54)

For G191–B2B, we have determined a relatively high upper abundance limit (about 100 times solar) for Mo (Sect. 6.4). This is well in agreement with a factor of about 100 – 1000 between the trans-iron element abundances in RE 0503–289 and G191–B2B. Like Mo, Kr, and Xe exhibit prominent lines in the UV spectra of RE 0503–289, but not in those of G191–B2B. To investigate on their abundances, we individually included Kr and Xe in our G191–B2B models and calculated theoretical profiles for all Kr and Xe lines that were identified in RE 0503–289 (Werner et al. 2012b; Rauch et al. 2015a). An upper Kr abundance limit of 10 times solar (1.09×10^{-6} by mass) is determined from lines of Kr^{VI}–VII simultaneously (Fig. 17). In the case of Xe, the intersystem lines Xe^{VII} $\lambda 995.51 \text{ \AA}$ ($5s^2 1S - 5s5p^3P^0$) and Xe^{VII} $\lambda 1077.12 \text{ \AA}$ ($5s5p^1P^0 - 5p^2 1D$) are very strong (Fig. 17) and require an upper Xe abundance limit of so-

lar to fade in the noise of the observation. However, this may be strongly underestimated because of the rudimentary Xe^{VII} model atom presently provided by TMAD. In that, only two Xe^{VII} lines with reliable oscillator strengths are known, namely, 0.245 for Xe^{VII} $\lambda 995.51 \text{ \AA}$ (Kernahan et al. 1980) and 0.810 for Xe^{VII} $\lambda 1077.12 \text{ \AA}$ (Biémont et al. 2007). Since, for the calculation of accurate NLTE occupation numbers of the atomic levels of an specific model ion, reliable transition probabilities are mandatory for the complete ion, the Xe^{VII} upper limit is regarded as uncertain. This issue is out of the scope of this paper but will be investigated in detail immediately after new Xe^{IV}–^{VII} transition probabilities become available. However, from the Xe^{VI} lines alone, we achieve an upper limit of 1.7×10^{-7} (10 times the solar value, Fig. 17).

7. Impact of diffusion on trans-iron elements

At almost the same $\log g$, RE 0503–289 has a significantly higher T_{eff} compared to that of G191–B2B ($T_{\text{eff}} = 70\,000 \text{ K}$, $\log g = 7.5$ vs. $T_{\text{eff}} = 60\,000 \text{ K}$, $\log g = 7.6$, respectively). Thus, the much stronger enrichment of the trans-iron elements in

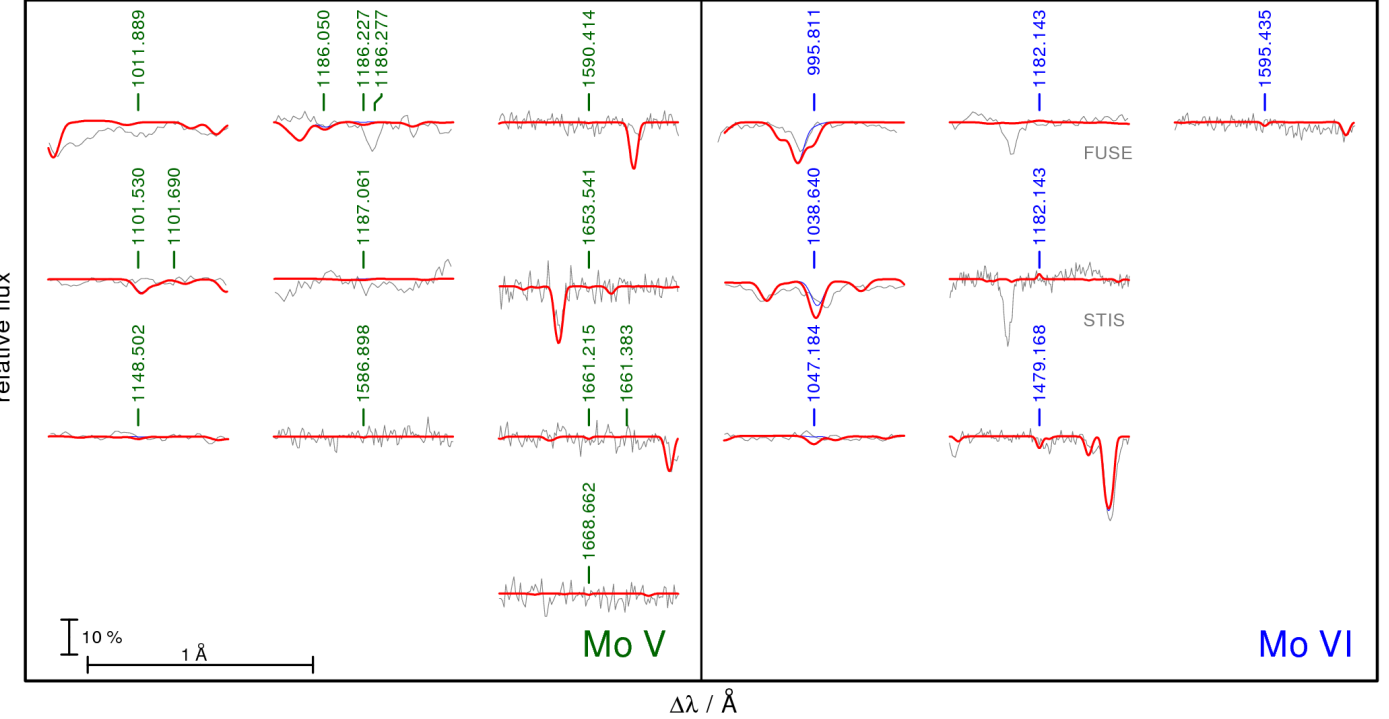


Fig. 16. Like Fig. 12 for G191–B2B. The thick red and thin blue spectra are calculated from models with photospheric Mo abundances of 5.3×10^{-6} and 5.3×10^{-7} (mass fractions, about 1000 and 100 times the solar value), respectively.

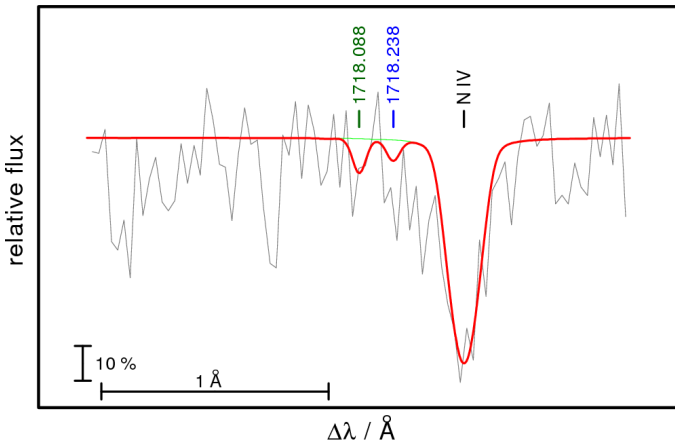


Fig. 14. Section of our HST/STIS observations of RE 0503–289 around $\text{N IV} \lambda 1718.55 \text{ \AA}$. The thick red and thin green lines show a comparison with theoretical spectra of two models with and without Mo, respectively. $\text{Mo V} \lambda 1718.088 \text{ \AA}$ and $\text{Mo VI} \lambda 1718.238 \text{ \AA}$ are marked.

RE 0503–289 (Fig. 18) may be the result of a more efficient radiative levitation. Therefore, we used the NGRT¹⁰ code (Dreizler & Wolff 1999; Schuh et al. 2002) to calculate diffusion models for both stars, using exactly the same model atoms for H, He, C, N, O, Ca, Sc, Ti, V, Cr, Mn, Fe, Co, Ni, Zn, Ga, Ge, As, Kr, Mo, Sn, Xe, and Ba, which were used for our chemically homogeneous TMAD models. For RE 0503–289, H was formally included in the calculation, but its abundance was fixed to 1.0×10^{-20} . Therefore, its contribution to the background opacity is negligible. Disregarding the fixed H abundance in RE 0503–289, the diffusion models differ only in T_{eff} and $\log g$.

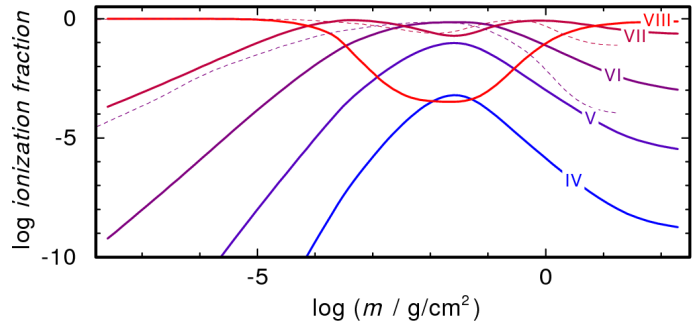


Fig. 15. Same as Fig. 10 for G191–B2B. For comparison, the dashed lines show the Mo VI+VII ionization fractions in the RE 0503–289 model.

The TMAD model atoms for As and Sn are presently rather rudimentary, especially as only a very few oscillator strengths are known. Restricting the radiative levitation calculation to include transitions with known oscillator strengths thus leads to an unrealistically small effect. We follow Rauch et al. (2013) and add all allowed line transitions in our As and Sn model atoms, using default f-values of 1. Therefore, the results of our diffusion models for these elements should be regarded as preliminary.

Figure 19 shows the calculated depth-dependent abundance profiles for Zn, Ga, Ge, As, Kr, Mo, Sn, Xe, and Ba. All these are strongly overabundant in the line-forming regions (Fig. 19). The predicted abundance profiles suggest abundance enhancements in RE 0503–289 relative to G191–B2B. This is qualitatively in agreement with the abundance patterns in Fig. 18, which were determined from our static TMAD models. However, whether it is possible to reach 2–3 dex should be demonstrated with advanced line-profile calculations in diffusive equilibrium. These would provide stringent constraints for suggested weak stellar winds (Chayer et al. 2005) and thin convective zones at the stel-

¹⁰ New Generation Radiative Transport

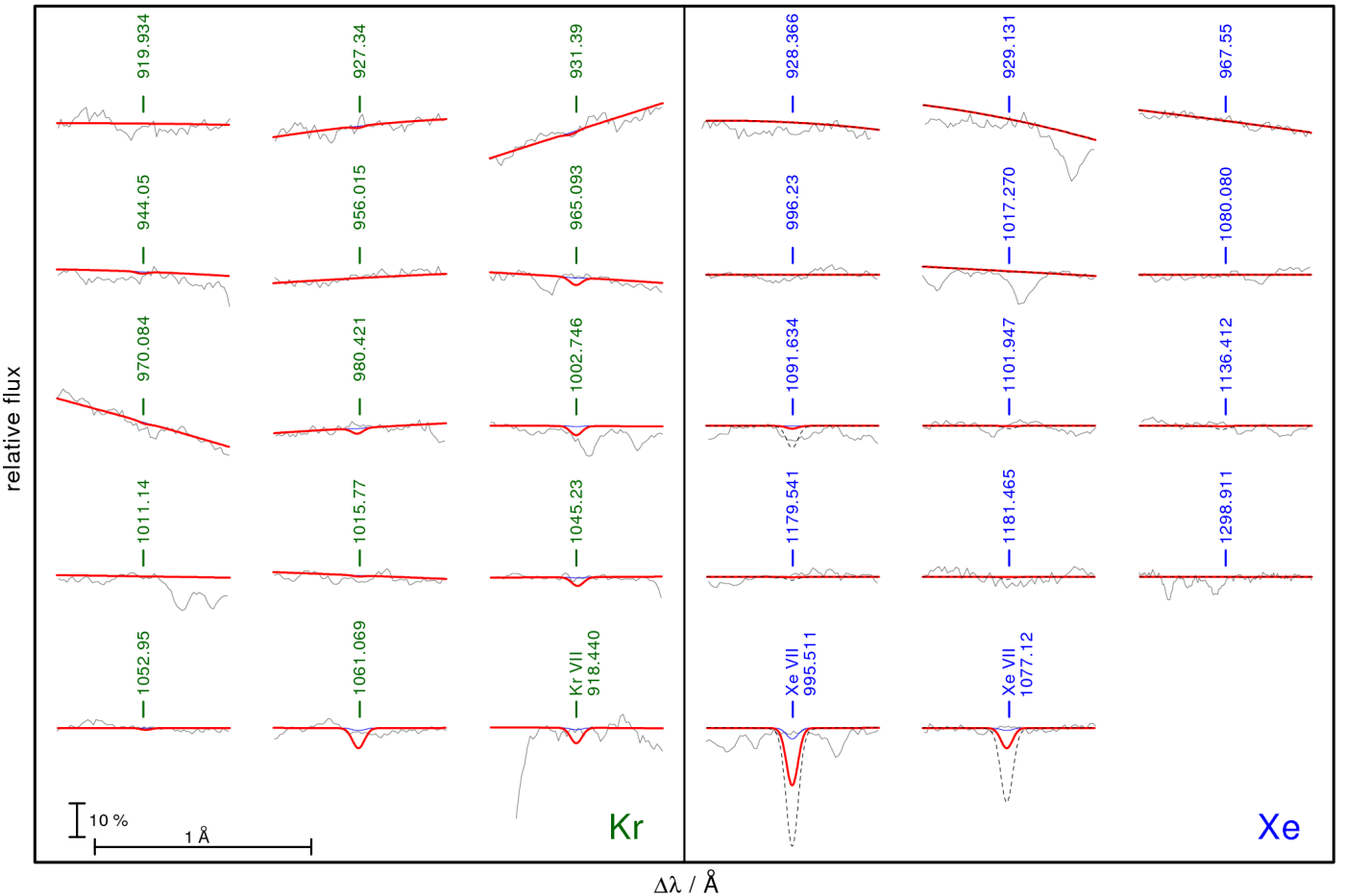


Fig. 17. Theoretical line profiles of Kr (left panel, 14 Kr vi lines and 1 Kr vii line) and Xe (right panel, 12 Xe vi and 2 Xe vii lines) compared to the observations of G191–B2B. The spectra are calculated from models with photospheric abundances (mass fractions) of Kr: 1.1×10^{-5} (thick red, 100 times solar) and 1.1×10^{-6} (thin blue, 10 times solar) and of Xe: 1.7×10^{-6} (dashed black, 100 times solar), 1.7×10^{-7} (thick red, 10 times solar), and 1.7×10^{-8} (thin blue, solar).

lar surface (Chayer et al. 2015), which might impact the interplay of radiative levitation and gravitational settling.

8. Results and conclusions

With our NLTE model-atmosphere package TMAP, we calculated new models for the DO-type white dwarf RE 0503–289 with molybdenum in addition. The Mo model atoms were constructed with newly calculated Mo iv–vii oscillator strengths. We have unambiguously identified 12 Mo v and nine Mo vi lines in the observed high-resolution UV spectra of RE 0503–289. The Mo v/Mo vi ionization equilibrium is well reproduced (Fig. 12). We determined a photospheric abundance of $\log \text{Mo} = -3.73 \pm 0.2$ (mass fraction $1.2 - 3.0 \times 10^{-4}$, 22 500–56 400 times the solar abundance). In addition, we determined the arsenic and tin abundances and derived $\log \text{As} = -5.08 \pm 0.2$ ($0.5 - 1.3 \times 10^{-5}$, about 300–1200 times solar) and $\log \text{Sn} = -3.69 \pm 0.2$ ($1.3 - 3.2 \times 10^{-4}$, about 14 300–35 200 times solar). These highly supersolar As, Mo, and Sn abundances agree well with the high abundances of other trans-iron elements in RE 0503–289 (Fig. 18).

G191–B2B does not exhibit Kr, Mo, and Xe lines in its UV spectrum. We investigated the strongest lines in the model and found upper limits for the abundances of Kr (1.1×10^{-6} , 10 times solar), Mo (5.3×10^{-7} , 100 times solar), and Xe (1.7×10^{-7} , 10 times solar). Whether radiative levitation yields abundances of

these elements that are consistent with observations should be demonstrated with advanced line-profile calculations in diffusive equilibrium, as depicted in Fig. 19. In addition, we determined the arsenic abundance and derived $\log \text{As} = -6.43 \pm 0.2$ ($2.3 - 5.9 \times 10^{-7}$, about 21–53 times solar).

The computation of reliable transition probabilities for Mo iv–vii was a prerequisite for the identification of Mo lines and the subsequent abundance determination. The hitherto known abundance pattern of RE 0503–289 (Fig. 18) indicates that other yet unidentified species should be detectable. Therefore, the precise evaluation of their laboratory spectra, i.e., the measurement of line wavelengths and strengths, as well as the determination of level energies and the subsequent calculation of transition probabilities are absolutely essential.

The example of the arsenic abundance determination (Sect. 6.1) had demonstrated that state-of-the-art NLTE stellar-atmosphere models are mandatory for the precise spectral analysis of hot stars.

Acknowledgements. TR and DH are supported by the German Aerospace Center (DLR, grants 05 OR 1402 and 50 OR 1501, respectively). The GAVO project had been supported by the Federal Ministry of Education and Research (BMBF) at Tübingen (05 AC 6 VTB, 05 AC 11 VTB) and is funded at Heidelberg (05 AC 11 VH3). Financial support from the Belgian FRS-FNRS is also acknowledged. PQ is research director of this organization. We thank our referee, Stéphane Vennes, for constructive criticism. Some of the data presented in this paper were obtained from the Mikulski Archive for Space Telescopes (MAST). STScI is operated by the Association of Universities for Research

Table 16. Same as Table 15, for G191–B2B.

Element	Mass Fraction	Number [X]	
H	9.99×10^{-1}	9.99×10^{-1}	0.132
He	$< 1.98 \times 10^{-5}$	$< 5.00 \times 10^{-6}$	< -4.099
C	6.31×10^{-6}	5.30×10^{-7}	-2.574
N	2.08×10^{-6}	1.50×10^{-7}	-2.522
O	1.90×10^{-5}	1.20×10^{-6}	-2.479
Al	1.12×10^{-5}	4.20×10^{-7}	-0.675
Si	5.29×10^{-5}	1.90×10^{-6}	-1.099
P	1.54×10^{-6}	5.00×10^{-8}	-0.579
S	5.72×10^{-6}	1.80×10^{-7}	-1.733
IG	1.78×10^{-6}	4.00×10^{-8}	-1.538
Fe	6.50×10^{-4}	1.17×10^{-5}	-0.269
Ni	3.84×10^{-5}	6.60×10^{-7}	-0.249
Zn	3.50×10^{-6}	5.40×10^{-8}	0.304
Ga	2.56×10^{-6}	3.70×10^{-8}	1.680
Ge	3.24×10^{-6}	4.50×10^{-8}	1.155
As	3.71×10^{-7}	5.00×10^{-9}	1.531
Kr	$< 1.09 \times 10^{-6}$	$< 1.31 \times 10^{-9}$	< 1.000
Mo	$< 5.33 \times 10^{-7}$	$< 5.60 \times 10^{-9}$	< 2.000
Sn	3.53×10^{-7}	3.00×10^{-9}	1.589
Xe	$< 1.67 \times 10^{-7}$	$< 1.28 \times 10^{-9}$	< 1.000
Ba	4.00×10^{-6}	2.94×10^{-8}	2.350

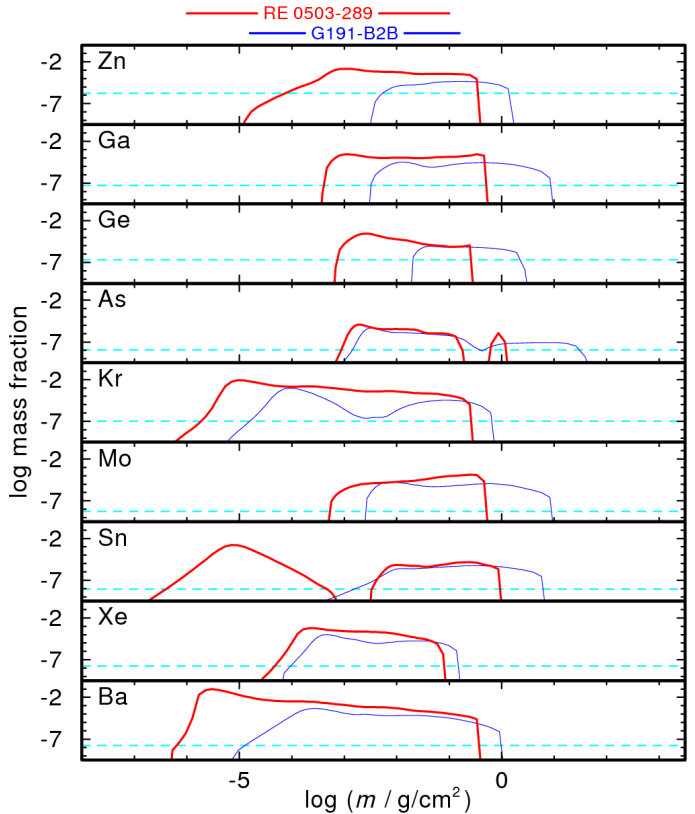


Fig. 19. Abundance profiles in our diffusion models for G191–B2B (thin blue) and RE 0503–289 (thick red). The dashed, horizontal lines indicate solar abundance values. The formation regions of UV lines in both models are indicated at the top.

in Astronomy, Inc., under NASA contract NAS5-26555. Support for MAST for non-HST data is provided by the NASA Office of Space Science via grant NNX09AF08G and by other grants and contracts. This research has made use of NASA’s Astrophysics Data System and the SIMBAD database, operated at CDS, Strasbourg, France. The TOSS service (<http://dc.g-vo.org/TOSS>) that provides weighted oscillator strengths and transition probabilities was constructed as part of the activities of the German Astrophysical Virtual Observatory.

References

- Asplund, M., Grevesse, N., Sauval, A. J., & Scott, P. 2009, *ARA&A*, 47, 481
- Biémont, É., Clar, M., Fivet, V., et al. 2007, *European Physical Journal D*, 44, 23
- Cabeza, M. I., Iglesias, L., Rico, F. R., & Kaufman, V. 1989, *Phys. Scr.*, 40, 457
- Chayer, P., Dupuis, J., & Kruk, J. W. 2015, in *Astronomical Society of the Pacific Conference Series*, Vol. 493, 19th European Workshop on White Dwarfs, ed. P. Dufour, P. Bergeron, & G. Fontaine, 3
- Chayer, P., Vennes, S., Dupuis, J., & Kruk, J. W. 2005, *ApJ*, 630, L169
- Cowan, R. D. 1981, *The theory of atomic structure and spectra* (Berkeley, CA, University of California Press)
- Cowley, C. R. 1970, *The theory of stellar spectra* (Gordon & Breach, New York)
- Cowley, C. R. 1971, *The Observatory*, 91, 139
- Curtis, L. J. & Theodosiou, C. E. 1989, *Phys. Rev. A*, 39, 605
- Dowler, P., Rixon, G., & Tody, D. 2010, *Table Access Protocol Version 1.0, IVOA Recommendation*
- Dreizler, S. & Werner, K. 1996, *A&A*, 314, 217
- Dreizler, S. & Wolff, B. 1999, *A&A*, 348, 189
- Fischer, C. F. 1977, *Journal of Physics B Atomic Molecular Physics*, 10, 1241
- Fraga, S., Karwowski, J., & Saxena, K. M. S. 1976, *Handbook of Atomic Data* (Elsevier, Amsterdam)
- Grevesse, N., Scott, P., Asplund, M., & Sauval, A. J. 2015, *A&A*, 573, A27
- Hubeny, I., Hummer, D. G., & Lanz, T. 1994, *A&A*, 282, 151
- Hummer, D. G. & Mihalas, D. 1988, *ApJ*, 331, 794
- Johnson, W. R., Kolb, D., & Huang, K.-N. 1983, *Atomic Data and Nuclear Data Tables*, 28, 333

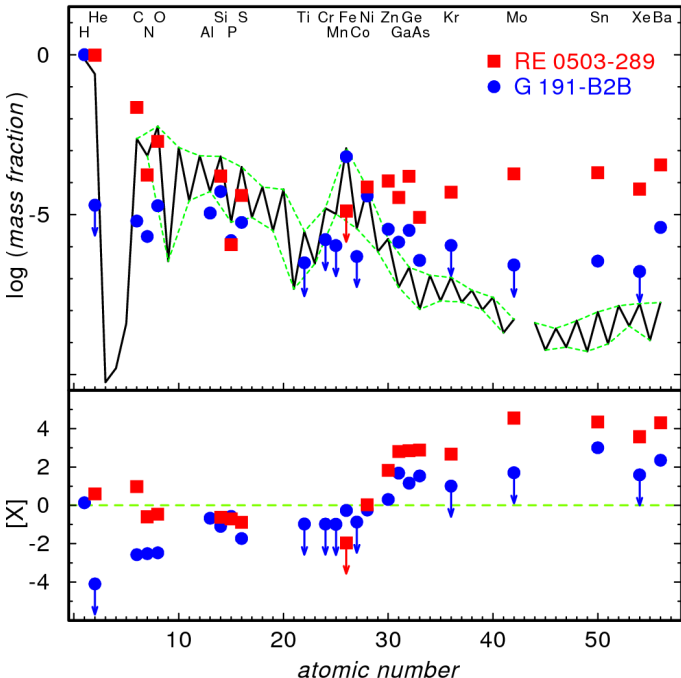


Fig. 18. Solar abundances (Asplund et al. 2009; Scott et al. 2015b,a; Grevesse et al. 2015, thick line; the dashed green lines connect the elements with even and with odd atomic number) compared with the determined photospheric abundances of G191–B2B (blue circles, Rauch et al. 2013) and RE 0503–289 (red squares, Dreizler & Werner 1996; Werner et al. 2012b; Rauch et al. 2013, 2014a,b, 2015a,b, and this work). Top panel: Abundances given as logarithmic mass fractions. Arrows indicate upper limits. Bottom panel: Abundance ratios to respective solar values, [X] denotes $\log(\text{fraction}/\text{solar fraction})$ of species X. The dashed green line indicates solar abundances.

- Kernahan, J. A., Pinnington, E. H., O'Neill, J. A., Bahr, J. L., & Donnelly, K. E. 1980, Journal of the Optical Society of America (1917-1983), 70, 1126
- McCook, G. P. & Sion, E. M. 1999a, ApJS, 121, 1
- McCook, G. P. & Sion, E. M. 1999b, VizieR Online Data Catalog, 3210, 0
- Migdalek, J. & Baylis, W. E. 1979, Journal of Physics B Atomic Molecular Physics, 12, 1113
- Moore, C. E. 1958, Atomic Energy Levels as Derived from the Analysis of Optical Spectra – Molybdenum through Lanthanum and Hafnium through Actinium (NIST)
- Morton, D. C. 2000, ApJS, 130, 403
- Osuna, P., Barbarisi, I., Salgado, J., & Arviset, C. 2005, in Astronomical Society of the Pacific Conference Series, Vol. 347, Astronomical Data Analysis Software and Systems XIV, ed. P. Shopbell, M. Britton, & R. Ebert, 198
- Osuna, P., Guainazzi, M., Salgado, J., Dubernet, M.-L., & Roueff, E. 2010, Simple Spectral Lines Data Model, IVOA Recommendation 2 Dec 2010
- Pinnington, E. H., Bahr, J. L., Kernahan, J. A., & Irwin, D. J. G. 1981, Journal of Physics B Atomic Molecular Physics, 14, 1291
- Quinet, P., Palmeri, P., Biémont, E., et al. 2002, J. Alloys Comp., 344, 255
- Quinet, P., Palmeri, P., Biémont, E., et al. 1999, MNRAS, 307, 934
- Rauch, T. 2012, ArXiv 1210.7636
- Rauch, T. & Deetjen, J. L. 2003, in Astronomical Society of the Pacific Conference Series, Vol. 288, Stellar Atmosphere Modeling, ed. I. Hubeny, D. Mihalas, & K. Werner, 103
- Rauch, T., Hoyer, D., Quinet, P., Gallardo, M., & Rainieri, M. 2015a, A&A, 577, A88
- Rauch, T., Werner, K., Biémont, É., Quinet, P., & Kruk, J. W. 2012, A&A, 546, A55
- Rauch, T., Werner, K., Bohlén, R., & Kruk, J. W. 2013, A&A, 560, A106
- Rauch, T., Werner, K., Quinet, P., & Kruk, J. W. 2014a, A&A, 564, A41
- Rauch, T., Werner, K., Quinet, P., & Kruk, J. W. 2014b, A&A, 566, A10
- Rauch, T., Werner, K., Quinet, P., & Kruk, J. W. 2015b, A&A, 577, A6
- Reader, J. 2010, Journal of Physics B Atomic Molecular Physics, 43, 074024
- Reader, J. & Tauheed, A. 2015, Journal of Physics B Atomic Molecular Physics, 48, 144001
- Salgado, J., Osuna, P., Guainazzi, M., et al. 2010, Simple Line Access Protocol, IVOA Recommendation 9 Dec 2010
- Schuh, S. L., Dreizler, S., & Wolff, B. 2002, A&A, 382, 164
- Scott, P., Asplund, M., Grevesse, N., Bergemann, M., & Sauval, A. J. 2015a, A&A, 573, A26
- Scott, P., Grevesse, N., Asplund, M., et al. 2015b, A&A, 573, A25
- Shirai, T., Sugar, J., Musgrove, A., & Wiese, W. L. 2000, Spectral Data for Highly Ionized Atoms: Ti, V, Cr, Mn, Fe, Co, Ni, Cu, Kr, and Mo (American Institute of Physics)
- Sugar, J. & Musgrove, A. 1988, Journal of Physical and Chemical Reference Data, 17, 155
- Vennes, S. & Lanz, T. 2001, ApJ, 553, 399
- Werner, K., Deetjen, J. L., Dreizler, S., et al. 2003, in Astronomical Society of the Pacific Conference Series, Vol. 288, Stellar Atmosphere Modeling, ed. I. Hubeny, D. Mihalas, & K. Werner, 31
- Werner, K., Dreizler, S., & Rauch, T. 2012a, TMAP: Tübingen NLTE Model-Atmosphere Package, Astrophysics Source Code Library
- Werner, K., Rauch, T., Ringat, E., & Kruk, J. W. 2012b, ApJ, 753, L7

Table 2. Radial parameters (in cm⁻¹) adopted for the calculations in Mo IV.

Configuration	Parameter	HFR	Fitted	Ratio	Note ^a
Even parity					
4d ³	E _{av}	17281	16028		
	F ² (4d,4d)	63593	53099	0.835	
	F ⁴ (4d,4d)	41828	36184	0.865	
	α	0	9		
	β	0	-491		
	ζ _{4d}	812	810	0.997	
4d ² 5s	E _{av}	75210	73187		
	F ² (4d,4d)	66028	53488	0.810	
	F ⁴ (4d,4d)	43601	36324	0.833	
	α	0	30		
	β	0	-417		
	ζ _{4d}	878	875	0.996	
	G ² (4d,5s)	15995	14485	0.906	
4d ² 6s	E _{av}	201514	200119		
	F ² (4d,4d)	67245	53932	0.802	
	F ⁴ (4d,4d)	44505	35007	0.787	
	α	0	45		
	β	0	-420		F
	ζ _{4d}	904	924	1.023	
	G ² (4d,6s)	3356	2624	0.782	
4d ² 5d	E _{av}	193759	193316		
	F ² (4d,4d)	67204	54471	0.811	
	F ⁴ (4d,4d)	44476	36658	0.824	
	α	0	31		
	β	0	-256		
	ζ _{4d}	903	924	1.024	
	ζ _{5d}	139	150	1.077	
	F ² (4d,5d)	14772	12432	0.842	
	F ⁴ (4d,5d)	6861	5749	0.838	
	G ⁰ (4d,5d)	4764	3206	0.673	
	G ² (4d,5d)	5093	3789	0.744	
	G ⁴ (4d,5d)	4081	3439	0.843	
Odd parity					
4d ² 5p	E _{av}	125149	124281		
	F ² (4d,4d)	66425	53851	0.811	
	F ⁴ (4d,4d)	43895	36220	0.825	
	α	0	33		
	β	0	-333		
	ζ _{4d}	888	930	1.048	
	ζ _{5p}	1801	2130	1.183	
	F ² (4d,5p)	25420	23019	0.906	
	G ¹ (4d,5p)	9987	9357	0.937	
	G ³ (4d,5p)	8792	8106	0.922	

^(a) F: parameter fixed in the fitting process.

Table 3. Radial parameters (in cm⁻¹) adopted for the calculations in Mo v.

Configuration	Parameter	HFR	Fitted	Ratio	Note ^a
Even parity					
4d ²	E_{av}	16700	15960		
	$F^2(4d,4d)$	67562	55311	0.819	
	$F^4(4d,4d)$	44738	35260	0.788	
	α	0	76		
	β	0	-166		
	ζ_{4d}	911	920	1.009	
4d5s	E_{av}	104520	99547		
	ζ_{4d}	976	982	1.005	
	$G^2(4d,5s)$	16390	14551	0.888	
4d6s	E_{av}	263493	256257		
	ζ_{4d}	1003	1022	1.019	
	$G^2(4d,6s)$	3729	3106	0.833	
4d5d	E_{av}	245631	239792		
	ζ_{4d}	1001	1016	1.015	
	ζ_{5d}	198	234	1.178	
	$F^2(4d,5d)$	18455	15120	0.819	
	$F^4(4d,5d)$	8872	7388	0.833	
	$G^0(4d,5d)$	5787	4043	0.699	
	$G^2(4d,5d)$	6372	5106	0.801	
	$G^4(4d,5d)$	5194	4146	0.798	
4d5g	E_{av}	335286	329641		
	ζ_{4d}	1012	1031	1.019	
	ζ_{5g}	1	1	1.000	F
	$F^2(4d,5g)$	6192	5389	0.870	
	$F^4(4d,5g)$	1861	1707	0.918	
	$G^2(4d,5g)$	1063	1139	1.071	R1
	$G^4(4d,5g)$	704	753	1.071	R1
	$G^6(4d,5g)$	518	555	1.071	R1
5s ²	E_{av}	213688	204228		
5p ²	E_{av}	332119	323949		
	$F^2(5p,5p)$	39738	41118	1.035	
	α	0	-621		
	ζ_{5p}	2540	3202	1.260	
5s5d	E_{av}	357810	349503		
	ζ_{5d}	219	219	1.000	F
	$G^2(5s,5d)$	19094	17185	0.900	F
5s6s	E_{av}	376977	370379		
	$G^0(5s,6s)$	3641	3277	0.900	F
Odd parity					
4d5p	E_{av}	162256	157254		
	ζ_{4d}	985	1075	1.091	R2
	ζ_{5p}	2318	2813	1.213	
	$F^2(4d,5p)$	28585	23914	0.837	
	$G^1(4d,5p)$	10632	10070	0.947	
	$G^3(4d,5p)$	9701	8409	0.867	
4d6p	E_{av}	287398	280416		
	ζ_{4d}	1004	1096	1.091	R2
	ζ_{6p}	971	1179	1.214	
	$F^2(4d,6p)$	10594	8043	0.759	
	$G^1(4d,6p)$	2868	1938	0.675	R3
	$G^3(4d,6p)$	2956	1995	0.675	R3
4d4f	E_{av}	256786	251161		
	ζ_{4d}	988	1077	1.091	R2
	ζ_{4f}	8	8	1.000	F
	$F^2(4d,4f)$	31387	26142	0.832	
	$F^4(4d,4f)$	17861	14862	0.832	

Table 3. continued.

Configuration	Parameter	HFR	Fitted	Ratio	Note ^a
4d5f	$G^1(4d,4f)$	31404	28322	0.901	
	$G^3(4d,4f)$	18764	16912	0.901	
	$G^5(4d,4f)$	13035	11745	0.901	
	E_{av}	325720	319198		
	ζ_{4d}	1001	1092	1.091	R2
	ζ_{5f}	5	5	1.000	F
	$F^2(4d,5f)$	13834	11607	0.839	
	$F^4(4d,5f)$	7809	6547	0.838	
	$G^1(4d,5f)$	13741	12541	0.913	
	$G^3(4d,5f)$	8630	7867	0.912	
4d6f	$G^5(4d,5f)$	6115	5570	0.911	
	E_{av}	363451	356835		
	ζ_{4d}	1007	1099	1.091	R2
	ζ_{6f}	3	3	1.000	F
	$F^2(4d,6f)$	7186	6050	0.842	
	$F^4(4d,6f)$	4053	3412	0.842	
	$G^1(4d,6f)$	6893	6546	0.950	
	$G^3(4d,6f)$	4448	4073	0.916	
	$G^5(4d,6f)$	3186	2917	0.915	
	E_{av}	386059	378193		
4d7f	ζ_{7f}	1010	1102	1.091	R2
	ζ_{7f}	2	2	1.000	F
	$F^2(4d,7f)$	4217	3557	0.843	
	$F^4(4d,7f)$	2381	2009	0.844	
	$G^1(4d,7f)$	3939	3621	0.919	
	$G^3(4d,7f)$	2584	2373	0.918	
	$G^5(4d,7f)$	1863	1711	0.918	
	E_{av}	400596	392685		
	ζ_{4d}	1011	1103	1.091	R2
	ζ_{8f}	1	1	1.000	F
4d8f	$F^2(4d,8f)$	2691	2272	0.844	
	$F^4(4d,8f)$	1522	1285	0.844	
	$G^1(4d,8f)$	2466	2271	0.921	
	$G^3(4d,8f)$	1635	1503	0.919	
	$G^5(4d,8f)$	1185	1088	0.918	
	E_{av}	410472	404023		
	ζ_{4d}	1012	1104	1.091	R2
	ζ_{9f}	1	1	1.000	F
	$F^2(4d,9f)$	1825	1552	0.850	F
	$F^4(4d,9f)$	1033	879	0.850	F
4d9f	$G^1(4d,9f)$	1650	1326	0.800	F
	$G^3(4d,9f)$	1102	884	0.800	F
	$G^5(4d,9f)$	801	642	0.800	F
	E_{av}	265407	258722		
	ζ_{5p}	2565	2961	1.154	
	$G^1(5s,5p)$	50976	39056	0.766	
	E_{av}	365788	356759		
	ζ_{4f}	11	11	1.000	F
	$G^3(5s,4f)$	28615	23484	0.821	
4p ⁵ 4d ³	E_{av}	340658	329068		
	$F^2(4d,4d)$	68193	53949	0.791	
	$F^4(4d,4d)$	45181	37828	0.837	
	α	0	-10		
	β	0	-127		
	ζ_{4p}	13353	13445	1.007	
	ζ_{4d}	936	878	0.938	
	$F^2(4p,4d)$	73694	64641	0.877	
	$G^1(4p,4d)$	92191	71050	0.771	

Table 3. continued.

Configuration	Parameter	HFR	Fitted	Ratio	Note ^a
G ³ (4p,4d)	56862	47299	0.832		

^a F: Fixed parameter value ; R1, R2, R3: ratios of these parameters were fixed in the fitting process.

Table 4. Radial parameters (in cm⁻¹) adopted for the calculations in Mo vi.

Configuration	Parameter	HFR	Fitted	Ratio	Note ^a
Even parity					
4d	E_{av}	6940	6979		
	ζ_{4d}	1014	1040	1.026	
5d	E_{av}	289239	285322		
	ζ_{5d}	264	303	1.148	
6d	E_{av}	391958	387186		
	ζ_{6d}	126	146	1.161	
7d	E_{av}	444684	440130		
	ζ_{7d}	71	83	1.170	
8d	E_{av}	475734	471318		
	ζ_{8d}	44	52	1.175	
5s	E_{av}	126902	124312		
6s	E_{av}	319460	314126		
7s	E_{av}	405700	400898		
8s	E_{av}	452302	447811		
5g	E_{av}	399240	395878		
	ζ_{5g}	1.4	1.4	1.000	F
6g	E_{av}	448202	444402		
	ζ_{6g}	0.7	0.7	1.000	F
7g	E_{av}	477706	473769		
	ζ_{7g}	0.4	0.4	1.000	F
8g	E_{av}	496846	492842		
	ζ_{8g}	0.3	0.3	1.000	F
7i	E_{av}	478466	474434		
	ζ_{7i}	0.2	0.2	1.000	F
8i	E_{av}	497360	493348		
	ζ_{8i}	0.1	0.1	1.000	F
Odd parity					
5p	E_{av}	191999	189199		
	ζ_{5p}	2857	3301	1.155	
6p	E_{av}	347659	342627		
	ζ_{6p}	1255	1382	1.102	
7p	E_{av}	420512	415898		
	ζ_{7p}	667	691	1.037	
8p	E_{av}	461055	456619		
	ζ_{8p}	397	407	1.024	
9p	E_{av}	486031	481747		
	ζ_{9p}	256	289	1.129	
10p	E_{av}	502531	498326		
	ζ_{10p}	174	179	1.024	
11p	E_{av}	514002	509824		
	ζ_{11p}	124	130	1.043	
4f	E_{av}	283752	279178		
	ζ_{4f}	15	15	1.000	F
5f	E_{av}	384116	378130		
	ζ_{5f}	10	10	1.000	F
6f	E_{av}	439000	433239		
	ζ_{6f}	5.7	5.7	1.000	F
7f	E_{av}	471803	466996		
	ζ_{7f}	3.6	3.6	1.000	F
8f	E_{av}	492861	488364		
	ζ_{8f}	2.4	2.4	1.000	F
9f	E_{av}	507147	502815		
	ζ_{9f}	1.7	1.7	1.000	F
6h	E_{av}	449115	445105		
	ζ_{6h}	0.5	0.5	1.000	F
7h	E_{av}	478275	474297		
	ζ_{7h}	0.3	0.3	1.000	F
8h	E_{av}	497230	493247		

Table 4. continued.

Configuration	Parameter	HFR	Fitted	Ratio	Note ^a
8k	ζ_{8h}	0.2	0.2	1.000	F
	E_{av}	497392	493378		
	ζ_{8k}	0.1	0.1	1.000	F
4p ⁵ 4d ²	E_{av}	335899	328744		
	$F^2(4d,4d)$	71670	59093	0.824	
	$F^4(4d,4d)$	47745	38616	0.809	
	α	0	17		
	β	0	-420		
	ζ_{4p}	13848	14202	1.026	
	ζ_{4d}	1037	1037	1.000	F
	$F^2(4p,4d)$	76913	66050	0.859	
	$G^1(4p,4d)$	96524	77164	0.799	
	$G^3(4p,4d)$	59818	49326	0.825	
4p ⁵ 4d5s	E_{av}	457444	450131		
	ζ_{4p}	14235	14483	1.017	
	ζ_{4d}	1101	1129	1.025	
	$F^2(4p,4d)$	78673	66507	0.845	
	$G^1(4p,4d)$	98887	88998	0.900	F
	$G^3(4p,4d)$	61423	55280	0.900	F
	$G^1(4p,5s)$	8984	7014	0.781	
	$G^2(4d,5s)$	16675	13729	0.823	
4f – 4p ⁵ 4d ²	$R^1(4p,4f;4d,4d)$	62948	54136	0.860	R1
	$R^3(4p,4f;4d,4d)$	36931	31762	0.860	R1
5f – 4p ⁵ 4d ²	$R^1(4p,5f;4d,4d)$	38112	29914	0.785	R2
	$R^3(4p,5f;4d,4d)$	23989	18829	0.785	R2
6f – 4p ⁵ 4d ²	$R^1(4p,6f;4d,4d)$	25591	23426	0.915	R3
	$R^3(4p,6f;4d,4d)$	16592	15188	0.915	R3

^a F: Fixed parameter value ; R1, R2, R3: ratios of these parameters were fixed in the fitting process.

Table 5. Radial parameters (in cm⁻¹) adopted for the calculations in Mo vii.

Configuration	Parameter	HFR	Fitted	Ratio	Note ^a
Even parity					
4p ⁶	E _{av}	0	21119		
4p ⁵ 5p	E _{av}	561281	562851		
	ζ _{4p}	14921	15363	1.030	
	ζ _{5p}	3488	4002	1.147	
	F ² (4p,5p)	29857	24371	0.816	
	G ⁰ (4p,5p)	6158	5332	0.866	
	G ² (4p,5p)	8430	7935	0.941	
4p ⁵ 4f	E _{av}	639783	641540		
	ζ _{4p}	14771	15580	1.055	
	ζ _{4f}	26	26	1.000	F
	F ² (4p,4f)	50260	41550	0.827	
	G ² (4p,4f)	39595	38768	0.979	
	G ⁴ (4p,4f)	26564	22964	0.864	
4p ⁵ 5f	E _{av}	779673	777325		
	ζ _{4p}	14910	14839	0.995	
	ζ _{5f}	16	16	1.000	F
	F ² (4p,5f)	20061	18055	0.900	F
	G ² (4p,5f)	14898	13408	0.900	F
	G ⁴ (4p,5f)	10403	9363	0.900	F
4s4p ⁶ 4d	E _{av}	598938	600309		
	ζ _{4d}	1152	1080	0.938	
	G ² (4s,4d)	75275	69544	0.924	
4p ⁴ 4d ²	E _{av}	677980	676885		
	ζ _{4p}	14606	15080	1.032	
Odd parity					
4p ⁵ 4d	E _{av}	333514	338837		
	ζ _{4p}	14422	14556	1.009	
	ζ _{4d}	1135	1208	1.063	
	F ² (4p,4d)	79809	71884	0.901	
	G ¹ (4p,4d)	100362	83374	0.831	
	G ³ (4p,4d)	62451	56668	0.907	
4p ⁵ 5d	E _{av}	671346	672809		
	ζ _{4p}	14913	15411	1.033	
	ζ _{5d}	334	377	1.127	
	F ² (4p,5d)	22803	18791	0.824	
	G ¹ (4p,5d)	11320	8210	0.725	
	G ³ (4p,5d)	8658	7930	0.916	
4p ⁵ 5s	E _{av}	488570	491951		
	ζ _{4p}	14829	15316	1.033	
	G ¹ (4p,5s)	9721	8535	0.878	
4p ⁵ 6s	E _{av}	717058	717580		
	ζ _{4p}	14952	15422	1.031	
	G ¹ (4p,6s)	3153	2754	0.874	
4p ⁵ 7s	E _{av}	823026	824426		
	ζ _{4p}	14988	14988	1.000	F
	G ¹ (4p,7s)	1479	1331	0.900	F
4p ⁵ 8s	E _{av}	881412	882412		
	ζ _{4p}	15003	15003	1.000	F
	G ¹ (4p,8s)	826	743	0.900	F
4p ⁵ 9s	E _{av}	917112	918112		
	ζ _{4p}	15010	15010	1.000	F
	G ¹ (4p,9s)	511	460	0.900	F
4p ⁵ 10s	E _{av}	940560	941960		
	ζ _{4p}	15015	15015	1.000	F
	G ¹ (4p,10s)	339	305	0.900	F
4p ⁵ 5g	E _{av}	801642	804198		

Table 5. continued.

Configuration	Parameter	HFR	Fitted	Ratio	Note ^a
	ζ_{4p}	15014	15478	1.031	
	ζ_{5g}	2.2	2.2	1.000	F
	$F^2(4p,5g)$	10237	9359	0.914	
	$G^3(4p,5g)$	1612	2007	1.245	
	$G^5(4p,5g)$	1141	1090	0.955	
4s4p ⁶ 5p	E_{av}	831694	831323		
	ζ_{5p}	3501	3501	1.000	F
	$G^1(4s,5p)$	8838	8527	0.965	

^a F: Fixed parameter value.

Table 6. Comparison between available experimental and calculated energy levels in Mo iv. Energies are given in cm⁻¹.

E_{exp}^a	E_{calc}^b	ΔE	J	Leading components (in %) in LS coupling ^c
Even parity				
0.00	-34	34	1.5	99 4d ³ 4F
778.02	742	36	2.5	99 4d ³ 4F
1759.76	1716	44	3.5	99 4d ³ 4F
2864.58	2817	48	4.5	98 4d ³ 4F
10330.59	10370	-39	1.5	82 4d ³ 4P + 16 4d ³ 2P
10337.77	10414	-76	0.5	92 4d ³ 4P + 8 4d ³ 2P
11580.50	11661	-80	3.5	99 4d ³ 2G
11611.99	11688	-76	2.5	99 4d ³ 4P
12310.80	12366	-55	4.5	83 4d ³ 2G + 15 4d ³ 2H
14175.62	14146	30	1.5	47 4d ³ 2P + 27 4d ³ 2D + 17 4d ³ 4P
14347.72	14124	224	0.5	91 4d ³ 2P + 8 4d ³ 4P
15995.13	15989	6	4.5	85 4d ³ 2H + 15 4d ³ 2G
16357.48	16326	31	5.5	100 4d ³ 2H
16809.32	17007	-198	2.5	80 4d ³ 2D + 17 4d ³ 2D
17107.35	17117	-10	1.5	46 4d ³ 2D + 36 4d ³ 2P + 14 4d ³ 2D
24787.03	24769	18	3.5	99 4d ³ 2F
25100.40	25075	25	2.5	98 4d ³ 2F
38922.29	38877	45	2.5	80 4d ³ 2D + 18 4d ³ 2D
39230.53	39234	-3	1.5	76 4d ³ 2D + 23 4d ³ 2D
60896.28	60933	-37	1.5	99 4d ² (³ F)5s 4F
61626.19	61665	-39	2.5	98 4d ² (³ F)5s 4F
62708.50	62744	-35	3.5	99 4d ² (³ F)5s 4F
64046.46	64077	-31	4.5	99 4d ² (³ F)5s 4F
69178.07	69126	52	2.5	93 4d ² (³ F)5s 2F
71358.31	71265	93	3.5	97 4d ² (³ F)5s 2F
71750.36	71680	70	0.5	99 4d ² (³ P)5s 4P
72162.82	72103	60	1.5	93 4d ² (³ P)5s 4P + 6 4d ² (¹ D)5s 2D
72236.20	72217	19	2.5	72 4d ² (³ P)5s 4P + 25 4d ² (¹ D)5s 2D
74008.77	74019	-10	1.5	89 4d ² (¹ D)5s 2D + 6 4d ² (³ P)5s 4P
74981.08	74977	4	2.5	69 4d ² (¹ D)5s 2D + 27 4d ² (³ P)5s 4P
79106.26	79132	-26	4.5	99 4d ² (¹ G)5s 2G
79193.56	79168	26	3.5	98 4d ² (¹ G)5s 2G
79898.80	79976	-77	0.5	97 4d ² (³ P)5s 2P
81052.21	81122	-70	1.5	95 4d ² (³ P)5s 2P
99783.80	99784	0	0.5	98 4d ² (¹ S)5s 2S
180788.80	180803	-14	2.5	64 4d ² (³ F)5d 4G + 32 4d ² (³ F)5d 2F
181502.72	181458	45	3.5	69 4d ² (³ F)5d 4H + 24 4d ² (³ F)5d 4G
182001.68	182007	-5	2.5	52 4d ² (³ F)5d 2F + 33 4d ² (³ F)5d 4G + 6 4d ² (³ F)5d 4D
182009.98	182053	-43	0.5	76 4d ² (³ F)5d 4D + 18 4d ² (³ F)5d 2P
182139.47	182091	48	3.5	72 4d ² (³ F)5d 4G + 22 4d ² (³ F)5d 4H
182451.72	182382	70	4.5	64 4d ² (³ F)5d 4H + 33 4d ² (³ F)5d 4G
182782.89	182767	16	1.5	91 4d ² (³ F)5d 4D
182924.12	183012	-88	3.5	71 4d ² (³ F)5d 2F + 9 4d ² (³ F)5d 4D + 7 4d ² (³ F)5d 2G
183312.22	183277	35	4.5	64 4d ² (³ F)5d 4G + 32 4d ² (³ F)5d 4H
183672.70	183612	61	5.5	64 4d ² (³ F)5d 4H + 33 4d ² (³ F)5d 4G
183697.92	183694	4	2.5	84 4d ² (³ F)5d 4D + 7 4d ² (³ F)5d 2F
184007.99	184108	-100	0.5	48 4d ² (³ F)5d 2P + 25 4d ² (³ F)5d 4P + 14 4d ² (³ F)5d 4D
184547.29	184527	20	5.5	64 4d ² (³ F)5d 4G + 35 4d ² (³ F)5d 4H
184987.76	185000	-12	3.5	84 4d ² (³ F)5d 4D + 6 4d ² (³ F)5d 2G + 5 4d ² (³ F)5d 2F
185253.43	185379	-126	1.5	44 4d ² (³ F)5d 4P + 38 4d ² (³ F)5d 2P + 8 4d ² (³ P)5d 4P
185283.50	185262	22	6.5	99 4d ² (³ F)5d 4H
185412.03	185440	-28	0.5	57 4d ² (³ F)5d 4P + 21 4d ² (³ F)5d 2P + 9 4d ² (³ P)5d 4P
186019.92	185978	42	3.5	65 4d ² (³ F)5d 2G + 13 4d ² (³ F)5d 2F + 8 4d ² (¹ D)5d 2G
186710.11	186571	139	4.5	85 4d ² (³ F)5d 2H + 10 4d ² (¹ G)5d 2H
186810.77	186908	-97	1.5	38 4d ² (³ F)5d 4P + 31 4d ² (³ F)5d 2P + 15 4d ² (³ F)5d 2D

Table 6. continued.

E_{exp}^a	E_{calc}^b	ΔE	J	Leading components (in %) in LS coupling ^c
186931.08	186976	-45	2.5	61 4d ² (³ F)5d ⁴ P + 15 4d ² (³ P)5d ⁴ P + 11 4d ² (³ F)5d ² D
187202.27	187228	-26	1.5	74 4d ² (³ F)5d ⁴ F + 11 4d ² (³ F)5d ² D + 8 4d ² (³ F)5d ² P
187237.70	187192	46	4.5	79 4d ² (³ F)5d ² G + 10 4d ² (¹ D)5d ² G
187688.42	187725	-37	1.5	44 4d ² (³ F)5d ² D + 18 4d ² (³ F)5d ⁴ F + 14 4d ² (¹ D)5d ² D
188032.96	188038	-5	2.5	82 4d ² (³ F)5d ⁴ F + 5 4d ² (³ F)5d ² D
188595.01	188641	-46	2.5	53 4d ² (³ F)5d ² D + 17 4d ² (¹ D)5d ² D + 12 4d ² (³ F)5d ⁴ P
188709.85	188615	95	5.5	86 4d ² (³ F)5d ² H + 10 4d ² (¹ G)5d ² H
188979.01	188982	-3	3.5	91 4d ² (³ F)5d ⁴ F
189966.52	189963	4	4.5	93 4d ² (³ F)5d ⁴ F
190833.77	190844	-10	1.5	96 4d ² (³ F)6s ⁴ F
191339.64	191333	7	2.5	77 4d ² (³ F)6s ⁴ F + 19 4d ² (³ F)6s ² F
191540.13	191524	16	1.5	59 4d ² (³ P)5d ² P + 35 4d ² (¹ D)5d ² P
191755.47	191757	-2	0.5	72 4d ² (¹ D)5d ² S + 17 4d ² (³ P)5d ² P
192578.85	192614	-35	3.5	88 4d ² (³ F)6s ⁴ F + 8 4d ² (³ F)6s ² F
192624.98	192633	-8	2.5	59 4d ² (¹ D)5d ² F + 20 4d ² (³ P)5d ² F + 8 4d ² (³ F)6s ² F
193319.52	193339	-19	3.5	55 4d ² (¹ D)5d ² F + 10 4d ² (³ P)5d ⁴ F + 10 4d ² (³ P)5d ² F
193379.15	193435	-56	2.5	71 4d ² (³ F)6s ² F + 15 4d ² (³ F)6s ⁴ F + 11 4d ² (¹ D)5d ² F
193462.57	193474	-12	0.5	42 4d ² (³ P)5d ² P + 27 4d ² (¹ D)5d ² P + 20 4d ² (¹ D)5d ² S
193779.78	193718	62	4.5	38 4d ² (¹ D)5d ² G + 31 4d ² (³ P)5d ⁴ F + 19 4d ² (³ F)6s ⁴ F
193815.29	193805	10	1.5	92 4d ² (³ P)5d ⁴ F
194100.67	194059	42	3.5	49 4d ² (¹ D)5d ² G + 20 4d ² (¹ D)5d ² F + 9 4d ² (³ P)5d ⁴ F
194235.12	194244	-9	2.5	85 4d ² (³ P)5d ⁴ F + 5 4d ² (³ P)5d ⁴ D
194296.81	194334	-37	4.5	78 4d ² (³ F)6s ⁴ F + 15 4d ² (¹ D)5d ² G
194970.47	194952	18	3.5	63 4d ² (³ P)5d ⁴ F + 10 4d ² (³ P)5d ² F + 8 4d ² (³ P)5d ⁴ D
195307.98	195298	10	1.5	72 4d ² (³ P)5d ⁴ D + 15 4d ² (¹ D)5d ² D + 6 4d ² (³ F)5d ² D
195454.02	195423	31	3.5	85 4d ² (³ F)6s ² F + 7 4d ² (³ F)6s ⁴ F
195672.25	195653	19	0.5	89 4d ² (³ P)5d ⁴ D + 6 4d ² (³ P)5d ² P
195740.65	195722	19	2.5	81 4d ² (³ P)5d ⁴ D + 5 4d ² (¹ D)5d ² D
196151.58	196092	60	2.5	44 4d ² (³ P)5d ² F + 36 4d ² (¹ G)5d ² F + 11 4d ² (¹ D)5d ² F
196179.49	196187	-8	1.5	30 4d ² (³ P)5d ⁴ P + 22 4d ² (¹ D)5d ² D + 13 4d ² (³ P)5d ⁴ D
196335.08	196332	3	4.5	61 4d ² (³ P)5d ⁴ F + 27 4d ² (¹ D)5d ² G + 7 4d ² (¹ G)5d ² G
196688.12	196670	18	3.5	39 4d ² (³ P)5d ⁴ D + 17 4d ² (¹ G)5d ² F + 11 4d ² (³ P)5d ² F
196828.31	196863	-35	3.5	38 4d ² (³ P)5d ⁴ D + 33 4d ² (³ P)5d ² F + 12 4d ² (¹ G)5d ² F
196953.22	196943	10	0.5	56 4d ² (³ P)5d ⁴ P + 17 4d ² (¹ D)5d ² P + 14 4d ² (³ P)5d ² P
197119.54	197108	12	2.5	55 4d ² (³ P)5d ⁴ P + 18 4d ² (¹ D)5d ² D + 15 4d ² (³ F)5d ⁴ P
197258.73	197292	-33	1.5	28 4d ² (³ P)5d ⁴ P + 17 4d ² (³ P)5d ² D + 14 4d ² (¹ D)5d ² D
198334.87	198425	-90	2.5	26 4d ² (³ P)5d ² D + 21 4d ² (¹ G)5d ² D + 18 4d ² (³ P)5d ⁴ P
198712.48	198686	26	0.5	39 4d ² (¹ D)5d ² P + 28 4d ² (³ P)5d ⁴ P + 17 4d ² (³ P)5d ² P
199069.41	199165	-96	3.5	86 4d ² (¹ G)5d ² G + 6 4d ² (³ F)5d ² G + 5 4d ² (¹ D)5d ² G
199087.52	199110	-22	1.5	24 4d ² (³ P)5d ² D + 20 4d ² (³ P)5d ⁴ P + 19 4d ² (¹ D)5d ² P
199229.00	199252	-23	2.5	35 4d ² (¹ D)5d ² D + 34 4d ² (³ P)5d ² D + 10 4d ² (¹ G)5d ² D
199394.17	199478	-84	4.5	73 4d ² (¹ G)5d ² G + 12 4d ² (¹ G)5d ² H + 7 4d ² (³ F)5d ² G
199722.50	199711	12	5.5	98 4d ² (¹ G)5d ² I
200086.20	200048	38	6.5	99 4d ² (¹ G)5d ² I
200189.54	200189	1	1.5	23 4d ² (¹ D)5d ² P + 18 4d ² (¹ D)5d ² D + 18 4d ² (³ P)5d ² D
201009.39	200995	14	4.5	76 4d ² (¹ G)5d ² H + 9 4d ² (³ F)5d ² H + 8 4d ² (¹ G)5d ² G
201022.59	200980	43	5.5	86 4d ² (¹ G)5d ² H + 11 4d ² (³ F)5d ² H
201355.10	201306	49	2.5	71 4d ² (¹ D)6s ² D + 26 4d ² (³ P)6s ⁴ P
201545.32	201488	57	1.5	79 4d ² (¹ D)6s ² D + 9 4d ² (³ P)6s ⁴ P + 8 4d ² (³ P)6s ² P
202114.64	202120	-5	0.5	95 4d ² (³ P)6s ⁴ P
202770.34	202787	-17	1.5	86 4d ² (³ P)6s ⁴ P + 8 4d ² (³ P)6s ² P + 5 4d ² (¹ D)6s ² D
203894.00	203890	4	0.5	96 4d ² (³ P)6s ² P
204269.40	204276	-7	2.5	47 4d ² (³ P)6s ⁴ P + 21 4d ² (¹ G)5d ² F + 15 4d ² (¹ D)6s ² D
204245.11	204148	97	3.5	59 4d ² (¹ G)5d ² F + 27 4d ² (³ P)5d ² F + 8 4d ² (¹ D)5d ² F
204426.26	204360	66	2.5	35 4d ² (¹ G)5d ² F + 27 4d ² (³ P)6s ⁴ P + 15 4d ² (³ P)5d ² F
205341.50	205360	-18	1.5	82 4d ² (³ P)6s ² P + 12 4d ² (¹ D)6s ² D
206861.16	206904	-43	1.5	65 4d ² (¹ G)5d ² D + 26 4d ² (³ P)5d ² D

Table 6. continued.

E_{exp}^a	E_{calc}^b	ΔE	J	Leading components (in %) in LS coupling ^c
207103.42	207142	-39	2.5	60 4d ² (¹ G)5d ² D + 29 4d ² (³ P)5d ² D
207561.80	207554	8	4.5	99 4d ² (¹ G)6s ² G
207567.86	207556	12	3.5	98 4d ² (¹ G)6s ² G
221465.60	221414	52	1.5	94 4d ² (¹ S)5d ² D
221491.80	221541	-49	2.5	96 4d ² (¹ S)5d ² D
Odd parity				
109415.25	109428	-13	2.5	81 4d ² (³ F)5p ⁴ G + 12 4d ² (³ F)5p ² F
111339.53	111334	6	3.5	90 4d ² (³ F)5p ⁴ G + 5 4d ² (³ F)5p ² F
111760.03	111727	33	1.5	76 4d ² (³ F)5p ⁴ F + 18 4d ² (³ F)5p ² D
112925.24	112962	-37	2.5	71 4d ² (³ F)5p ⁴ F + 12 4d ² (³ F)5p ² D + 7 4d ² (³ F)5p ⁴ D
113443.02	113424	19	4.5	92 4d ² (³ F)5p ⁴ G + 6 4d ² (³ F)5p ⁴ F
113984.98	114010	-25	2.5	39 4d ² (³ F)5p ² F + 21 4d ² (³ F)5p ⁴ F + 16 4d ² (³ F)5p ⁴ G
114624.49	114561	63	3.5	90 4d ² (³ F)5p ⁴ F
114708.24	114756	-48	1.5	42 4d ² (³ F)5p ² D + 22 4d ² (³ F)5p ⁴ F + 16 4d ² (³ F)5p ⁴ D
115762.16	115869	-107	3.5	62 4d ² (³ F)5p ² F + 23 4d ² (³ F)5p ⁴ D + 6 4d ² (³ F)5p ⁴ G
115789.36	115729	60	0.5	79 4d ² (³ F)5p ⁴ D + 17 4d ² (³ P)5p ⁴ D
115881.12	115816	65	5.5	99 4d ² (³ F)5p ⁴ G
115961.91	115897	65	4.5	84 4d ² (³ F)5p ⁴ F + 7 4d ² (³ F)5p ² G + 7 4d ² (³ F)5p ⁴ G
116583.82	116641	-57	2.5	46 4d ² (³ F)5p ⁴ D + 17 4d ² (³ F)5p ² F + 14 4d ² (³ F)5p ² D
116586.00	116618	-32	1.5	61 4d ² (³ F)5p ⁴ D + 16 4d ² (³ P)5p ⁴ D + 12 4d ² (³ F)5p ² D
117604.08	117752	-148	2.5	31 4d ² (³ F)5p ² D + 28 4d ² (³ F)5p ⁴ D + 17 4d ² (³ P)5p ² D
117922.63	118177	-255	0.5	92 4d ² (³ P)5p ² S
118080.17	118097	-17	3.5	58 4d ² (³ F)5p ⁴ D + 15 4d ² (³ F)5p ² F + 10 4d ² (³ P)5p ⁴ D
119002.33	118975	27	3.5	77 4d ² (³ F)5p ² G + 13 4d ² (¹ G)5p ² G
120645.02	120664	-19	4.5	72 4d ² (³ F)5p ² G + 15 4d ² (¹ G)5p ² G + 11 4d ² (³ F)5p ⁴ F
120823.46	120749	74	1.5	69 4d ² (³ P)5p ⁴ S + 22 4d ² (¹ D)5p ² P
122419.26	122399	20	0.5	80 4d ² (³ P)5p ⁴ D + 17 4d ² (³ F)5p ⁴ D
122808.84	122887	-78	1.5	31 4d ² (¹ D)5p ² P + 21 4d ² (³ P)5p ⁴ S + 19 4d ² (³ P)5p ⁴ D
123432.84	123426	7	1.5	61 4d ² (³ P)5p ⁴ D + 19 4d ² (¹ D)5p ² P + 8 4d ² (³ F)5p ⁴ D
123534.18	123406	128	2.5	59 4d ² (¹ D)5p ² F + 15 4d ² (³ F)5p ² F + 8 4d ² (³ P)5p ⁴ D
124741.62	124818	-76	0.5	82 4d ² (¹ D)5p ² P + 12 4d ² (³ P)5p ⁴ P
124789.75	124723	67	2.5	70 4d ² (³ P)5p ⁴ D + 14 4d ² (¹ D)5p ² F + 9 4d ² (³ F)5p ⁴ D
124947.54	124828	120	3.5	43 4d ² (¹ D)5p ² F + 20 4d ² (¹ G)5p ² G + 16 4d ² (³ P)5p ⁴ D
126243.19	126330	-87	1.5	44 4d ² (¹ D)5p ² D + 20 4d ² (¹ D)5p ² P + 18 4d ² (³ P)5p ⁴ P
126416.33	126342	74	3.5	55 4d ² (³ P)5p ⁴ D + 29 4d ² (¹ G)5p ² G + 5 4d ² (³ F)5p ² G
126716.64	126760	-43	2.5	53 4d ² (¹ D)5p ² D + 29 4d ² (³ P)5p ⁴ P + 6 4d ² (³ F)5p ² D
126760.46	126707	53	0.5	83 4d ² (³ P)5p ⁴ P + 9 4d ² (¹ D)5p ² P + 6 4d ² (³ P)5p ² S
126999.09	126897	102	4.5	70 4d ² (¹ G)5p ² G + 19 4d ² (³ F)5p ² G + 10 4d ² (¹ G)5p ² H
127181.20	127129	52	1.5	77 4d ² (³ P)5p ⁴ P + 18 4d ² (¹ D)5p ² D
127728.82	127634	95	3.5	33 4d ² (¹ G)5p ² G + 32 4d ² (¹ D)5p ² F + 17 4d ² (³ P)5p ⁴ D
128897.78	128862	36	2.5	64 4d ² (³ P)5p ⁴ P + 32 4d ² (¹ D)5p ² D
130149.35	129987	162	4.5	87 4d ² (¹ G)5p ² H + 12 4d ² (¹ G)5p ² G
131699.83	131641	59	1.5	65 4d ² (³ P)5p ² D + 13 4d ² (³ P)5p ² P + 13 4d ² (³ F)5p ² D
132012.37	131849	163	5.5	99 4d ² (¹ G)5p ² H
132219.07	132241	-22	2.5	70 4d ² (³ P)5p ² D + 20 4d ² (³ F)5p ² D
133362.00	133350	12	0.5	92 4d ² (³ P)5p ² P
134242.50	134223	20	1.5	79 4d ² (³ P)5p ² P + 9 4d ² (³ P)5p ² D
134951.06	135198	-247	3.5	90 4d ² (¹ G)5p ² F
136324.44	136602	-278	2.5	94 4d ² (¹ G)5p ² F
150069.22	150096	-27	0.5	92 4d ² (¹ S)5p ² P
152757.31	152729	28	1.5	95 4d ² (¹ S)5p ² P

^(a) From Sugar & Musgrave (1988) and Cabeza et al. (1989).^(b) This work.^(c) Only the first three components that are larger than 5% are given.

Table 7. Comparison between available experimental and calculated energy levels in Mo v. Energies are given in cm⁻¹.

E_{exp}^a	E_{calc}^b	ΔE	J	Leading components (in %) in LS coupling ^c
Even parity				
0.00	12	-12	2	97 4d ² ³ F
1577.17	1577	0	3	99 4d ² ³ F
3357.08	3345	12	4	98 4d ² ³ F
10190.11	10186	4	2	76 4d ² ¹ D + 21 4d ² ³ P
11161.31	11149	12	0	98 4d ² ³ P
11806.93	11808	-1	1	99 4d ² ³ P
13408.30	13423	-15	2	78 4d ² ³ P + 21 4d ² ¹ D
16353.36	16353	0	4	98 4d ² ¹ G
37737.83	37738	0	0	98 4d ² ¹ S
92380.54	92375	5	1	99 4d5s ³ D
93111.40	93118	-7	2	95 4d5s ³ D
94835.44	94834	1	3	99 4d5s ³ D
99380.40	99380	0	2	95 4d5s ¹ D
199050.87	199051	0	0	96 5s ² ¹ S
232561.12	232576	-15	3	79 4d5d ¹ F + 11 4d5d ³ G + 8 4d5d ³ D
233190.31	233194	-4	1	81 4d5d ³ D + 18 4d5d ¹ P
234252.45	234252	0	2	97 4d5d ³ D
234490.48	234468	22	3	82 4d5d ³ G + 10 4d5d ³ D + 5 4d5d ¹ F
235496.01	235472	24	4	97 4d5d ³ G
235634.96	235640	-5	3	80 4d5d ³ D + 14 4d5d ¹ F + 5 4d5d ³ G
236002.02	236033	-31	1	73 4d5d ¹ P + 18 4d5d ³ D + 7 4d5d ³ S
237204.53	237183	22	5	99 4d5d ³ G
237759.53	237755	5	2	93 4d5d ³ F + 5 4d5d ¹ D
239068.95	239071	-2	3	96 4d5d ³ F
239188.82	239203	-14	1	88 4d5d ³ S + 8 4d5d ¹ P
240109.61	240111	-1	4	96 4d5d ³ F
241964.75	241971	-6	2	70 4d5d ¹ D + 23 4d5d ³ P
242161.93	242171	-9	0	96 4d5d ³ P
242971.44	242962	9	1	95 4d5d ³ P
243954.32	243952	2	2	75 4d5d ³ P + 23 4d5d ¹ D
244170.15	244167	3	4	96 4d5d ¹ G
251017.96	251018	0	0	94 4d5d ¹ S
254125.95	254125	1	1	100 4d6s ³ D
254464.98	254466	-1	2	77 4d6s ³ D + 23 4d6s ¹ D
256676.48	256677	-1	3	100 4d6s ³ D
257442.81	257442	1	2	77 4d6s ¹ D + 23 4d6s ³ D
314344.75	314213	131	0	76 5p ² ³ P + 18 4d6d ³ P
320344.53	320431	-86	2	64 4d6d ¹ D + 11 5p ² ¹ D + 8 4d6d ³ P
320917.27	321522	-605	1	68 4d6d ³ P + 26 5p ² ³ P
323777.46	323661	116	2	50 5p ² ³ P + 32 4d6d ³ P + 8 5p ² ¹ D
327070.61	327063	8	5	37 4d5g ¹ H + 37 4d5g ³ H + 25 4d5g ³ G
327141.68	327129	13	4	74 4d5g ³ H + 16 4d5g ³ G + 10 4d5g ¹ G
327386.30	327370	16	3	63 4d5g ³ G + 22 4d5g ¹ F + 15 4d5g ³ F
327436.40	327436	0	4	37 4d5g ³ F + 32 4d5g ³ G + 30 4d5g ¹ G
327859.16	327879	-20	5	70 4d5g ³ I + 15 4d5g ³ H + 14 4d5g ¹ H
327995.37	328035	-40	6	42 4d5g ³ I + 32 4d5g ³ H + 26 4d5g ¹ I
328234.03	328216	18	3	47 4d5g ³ D + 30 4d5g ³ F + 22 4d5g ¹ F
328265.06	328263	2	2	54 4d5g ³ F + 26 4d5g ¹ D + 19 4d5g ³ D
329713.88	329715	-1	5	68 4d5g ³ G + 26 4d5g ¹ H
329795.97	329799	-3	4	39 4d5g ³ G + 34 4d5g ¹ G + 24 4d5g ³ H
329810.15	329812	-2	5	44 4d5g ³ H + 26 4d5g ³ I + 23 4d5g ¹ H
329897.53	329906	-8	6	68 4d5g ³ H + 24 4d5g ³ I + 8 4d5g ¹ I
330052.53	330030	23	3	37 4d5g ¹ F + 37 4d5g ³ G + 26 4d5g ³ F
330100.52	330090	11	4	61 4d5g ³ F + 26 4d5g ¹ G + 13 4d5g ³ G
330656.07	330687	-31	7	100 4d5g ³ I

Table 7. continued.

E_{exp}^a	E_{calc}^b	ΔE	J	Leading components (in %) in LS coupling ^c
330667.37	330642	25	3	52 4d5g ³ D + 29 4d5g ³ F + 19 4d5g ¹ F
330699.70	330689	11	2	46 4d5g ³ F + 28 4d5g ³ D + 25 4d5g ¹ D
330878.23	330943	-65	6	65 4d5g ¹ I + 34 4d5g ³ I
331233.74	331189	45	1	99 4d5g ³ D
331263.46	331262	1	2	51 4d5g ³ D + 47 4d5g ¹ D
346764.00	346827	-63	1	98 5s5d ³ D
347006.81	347023	-16	2	98 5s5d ³ D
347408.70	347331	78	3	98 5s5d ³ D
349643.40	349647	-4	0	85 5p ² ¹ S + 7 4d6d ¹ S
368808.38	368808	0	1	100 5s6s ³ S
Odd parity				
146976.75	146976	1	2	53 4d5p ¹ D + 42 4d5p ³ F
148948.66	148841	108	1	93 4d5p ³ D
150345.79	150449	-103	2	48 4d5p ³ D + 27 4d5p ¹ D + 18 4d5p ³ F
151195.14	151178	17	3	69 4d5p ³ F + 28 4d5p ³ D
151213.20	151163	50	2	45 4d5p ³ D + 39 4d5p ³ F + 15 4d5p ¹ D
153039.67	153077	-37	3	67 4d5p ³ D + 30 4d5p ³ F
155032.33	155054	-22	4	99 4d5p ³ F
156616.49	156549	67	1	84 4d5p ³ P + 11 4d5p ¹ P
157059.18	157034	25	0	99 4d5p ³ P
157851.46	157928	-77	2	92 4d5p ³ P
159856.69	159923	-66	3	94 4d5p ¹ F
162257.12	162221	36	1	83 4d5p ¹ P + 13 4d5p ³ P
237482.33	237668	-186	4	83 4d4f ¹ G + 7 4d4f ³ F
239392.83	239263	130	2	82 4d4f ³ F + 13 4d4f ¹ D
239949.69	240199	-249	4	80 4d4f ³ H + 13 4d4f ³ F
240004.70	239937	68	3	90 4d4f ³ F
240725.04	241156	-431	5	95 4d4f ³ H
240878.05	241046	-168	4	72 4d4f ³ F + 12 4d4f ³ H + 11 4d4f ¹ G
241752.33	242135	-383	2	79 4d4f ¹ D + 12 4d4f ³ F
241972.61	242613	-640	6	98 4d4f ³ H
243408.59	242726	683	3	82 4d4f ³ G + 8 4p ⁵ 4d ³ (² H) ³ G
244626.80	244102	525	4	83 4d4f ³ G + 7 4p ⁵ 4d ³ (² H) ³ G
245600.22	245199	401	5	87 4d4f ³ G + 7 4p ⁵ 4d ³ (² H) ³ G
246619.40	246889	-270	0	67 5s5p ³ P + 31 4d4f ³ P
246799.61	246586	214	1	54 4d4f ³ D + 22 4d4f ³ P + 14 5s5p ³ P
247090.71	246813	278	2	59 4d4f ³ D + 27 4d4f ³ P
247687.61	247406	282	3	83 4d4f ³ D + 6 4d4f ¹ F
247932.56	247852	81	1	36 5s5p ³ P + 34 4d4f ³ D + 24 4d4f ³ P
248745.05	248576	169	2	47 4d4f ³ P + 31 4d4f ³ D + 15 5s5p ³ P
250990.91	250913	78	3	85 4d4f ¹ F + 6 4d4f ³ D
252463.44	252209	254	0	63 4d4f ³ P + 33 5s5p ³ P
252648.40	252507	141	1	48 4d4f ³ P + 47 5s5p ³ P
254209.83	254298	-88	2	79 5s5p ³ P + 18 4d4f ³ P
255941.37	255888	53	1	80 4d4f ¹ P + 14 5s5p ¹ P
259254.51	259880	-625	5	92 4d4f ¹ H
275024.25	274831	193	1	46 5s5p ¹ P + 31 4d6p ¹ P + 12 4d6p ³ D
276470.33	276478	-8	2	45 4d6p ³ F + 41 4d6p ¹ D + 12 4d6p ³ D
277187.91	277191	-3	1	85 4d6p ³ D + 11 5s5p ¹ P
278004.86	277960	45	2	60 4d6p ³ D + 35 4d6p ³ F
278999.30	278971	28	3	68 4d6p ³ F + 16 4d6p ³ D + 16 4d6p ¹ F
279060.06	279214	-154	2	44 4d6p ¹ D + 27 4d6p ³ D + 18 4d6p ³ F
279478.11	279478	0	3	65 4d6p ³ D + 27 4d6p ³ F + 7 4d6p ¹ F
280277.20	280478	-201	4	38 4p ⁵ 4d ³ (⁴ P) ⁵ D + 33 4p ⁵ 4d ³ (⁴ F) ⁵ D + 26 4p ⁵ 4d ³ (⁴ F) ⁵ F
280279.09	280081	198	0	99 4d6p ³ P
280505.47	280414	91	1	92 4d6p ³ P

Table 7. continued.

E_{exp}^a	E_{calc}^b	ΔE	J	Leading components (in %) in LS coupling ^c
281268.15	281479	-211	4	100 4d6p ³ F
281996.44	281709	287	3	75 4d6p ¹ F + 19 4d6p ³ D
282057.02	282025	32	2	88 4d6p ³ P + 10 4d6p ¹ D
285619.22	286160	-541	1	65 4d6p ¹ P + 19 5s5p ¹ P + 6 4d4f ¹ P
287427.80	287135	293	4	52 4p ⁵ 4d ³ (⁴ F) ⁵ F + 19 4p ⁵ 4d ³ (⁴ P) ⁵ D + 17 4p ⁵ 4d ³ (⁴ F) ⁵ G
287471.40	287899	-428	3	51 4p ⁵ 4d ³ (⁴ F) ⁵ F + 15 4p ⁵ 4d ³ (⁴ P) ⁵ D + 13 4p ⁵ 4d ³ (⁴ F) ⁵ G
287818.70	287881	-62	1	76 4p ⁵ 4d ³ (⁴ F) ⁵ F + 6 4p ⁵ 4d ³ (⁴ F) ⁵ D + 5 4p ⁵ 4d ³ (⁴ F) ³ D
287997.70	287965	33	2	57 4p ⁵ 4d ³ (⁴ F) ⁵ F + 10 4p ⁵ 4d ³ (⁴ F) ⁵ D + 9 4p ⁵ 4d ³ (⁴ P) ⁵ D
294230.46	294553	-323	2	46 4p ⁵ 4d ³ (² G) ³ F + 20 4p ⁵ 4d ³ (⁴ F) ³ F + 9 4p ⁵ 4d ³ (⁴ F) ⁵ G
294925.20	294691	234	5	66 4p ⁵ 4d ³ (⁴ F) ⁵ G + 15 4p ⁵ 4d ³ (⁴ F) ⁵ F + 10 4p ⁵ 4d ³ (⁴ F) ³ G
296151.14	296102	49	4	36 4p ⁵ 4d ³ (⁴ F) ⁵ G + 17 4p ⁵ 4d ³ (² H) ³ G + 16 4p ⁵ 4d ³ (⁴ F) ³ G
296191.62	296489	-297	3	31 4p ⁵ 4d ³ (² G) ³ F + 19 4p ⁵ 4d ³ (² H) ³ G + 10 4p ⁵ 4d ³ (⁴ F) ³ F
297369.77	297386	-16	3	32 4p ⁵ 4d ³ (⁴ F) ⁵ G + 11 4p ⁵ 4d ³ (⁴ F) ³ G
297428.25	297454	-26	2	41 4p ⁵ 4d ³ (² P) ³ P + 13 4p ⁵ 4d ³ (² D) ³ P + 12 4p ⁵ 4d ³ (² D) ³ D
298928.26	298886	42	4	29 4p ⁵ 4d ³ (² G) ³ F + 14 4p ⁵ 4d ³ (⁴ F) ⁵ G + 12 4p ⁵ 4d ³ (⁴ F) ³ F
299310.36	299268	42	1	34 4p ⁵ 4d ³ (² P) ³ P + 20 4p ⁵ 4d ³ (² D) ³ P + 10 4p ⁵ 4d ³ (² D) ³ D
299916.96	299865	52	3	32 4p ⁵ 4d ³ (² D) ³ D + 13 4p ⁵ 4d ³ (² P) ³ D + 12 4p ⁵ 4d ³ (⁴ F) ³ D
301540.26	300802	738	5	27 4p ⁵ 4d ³ (² F) ³ G + 21 4p ⁵ 4d ³ (² H) ³ G + 19 4p ⁵ 4d ³ (² G) ³ G
301775.31	301725	50	4	19 4p ⁵ 4d ³ (⁴ F) ⁵ G + 14 4p ⁵ 4d ³ (² G) ¹ G + 11 4p ⁵ 4d ³ (² H) ¹ G
301935.30	301818	117	0	41 4p ⁵ 4d ³ (² P) ³ P + 27 4p ⁵ 4d ³ (² D) ³ P + 14 4p ⁵ 4d ³ (² D) ³ P
302869.95	302640	230	2	20 4p ⁵ 4d ³ (² D) ³ D + 18 4p ⁵ 4d ³ (² P) ³ P + 15 4p ⁵ 4d ³ (² P) ³ D
303813.31	303776	37	1	24 4p ⁵ 4d ³ (² D) ³ D + 14 4p ⁵ 4d ³ (² P) ³ P + 13 4p ⁵ 4d ³ (² F) ³ D
303955.54	303688	268	3	36 4p ⁵ 4d ³ (⁴ F) ⁵ G + 20 4d5f ³ G + 12 4p ⁵ 4d ³ (² H) ³ G
304727.38	304885	-158	3	38 4p ⁵ 4d ³ (² P) ³ D + 27 4d5f ³ D + 7 4p ⁵ 4d ³ (² F) ³ D
304828.89	304592	237	6	82 4p ⁵ 4d ³ (² G) ³ H + 9 4p ⁵ 4d ³ (² H) ³ I
304831.60	304532	300	2	73 4p ⁵ 4d ³ (⁴ F) ⁵ G + 11 4p ⁵ 4d ³ (² G) ³ F
306037.34	306133	-96	4	25 4d5f ³ G + 13 4d5f ¹ G + 12 4p ⁵ 4d ³ (² G) ¹ G
306992.33	306846	146	5	49 4p ⁵ 4d ³ (² G) ³ H + 18 4d5f ³ G + 8 4d5f ³ H
307588.25	307218	370	4	55 4p ⁵ 4d ³ (² D) ³ F + 21 4p ⁵ 4d ³ (² F) ³ F
307863.79	307636	228	2	35 4d5f ³ D + 22 4p ⁵ 4d ³ (² P) ³ D + 13 4p ⁵ 4d ³ (² F) ³ D
308939.76	308963	-23	3	24 4d5f ¹ F + 17 4p ⁵ 4d ³ (² D) ³ F + 13 4p ⁵ 4d ³ (² D) ¹ F
310475.83	310307	169	1	32 4d5f ³ D + 21 4p ⁵ 4d ³ (² P) ³ D + 8 4p ⁵ 4d ³ (² F) ³ D
310668.20	310405	263	3	22 4d5f ³ G + 20 4d5f ³ F + 16 4p ⁵ 4d ³ (² G) ³ G
311070.16	311095	-25	4	27 4d5f ³ H + 22 4d5f ¹ G + 8 4p ⁵ 4d ³ (² G) ³ G
311351.67	311402	-50	2	52 4d5f ¹ D + 11 4d5f ³ F + 6 4d5f ³ P
311959.68	311636	324	5	36 4d5f ³ G + 26 4p ⁵ 4d ³ (² G) ³ G + 16 4p ⁵ 4d ³ (² G) ¹ H
312298.30	312238	60	3	73 4p ⁵ 4d ³ (⁴ P) ⁵ P + 10 4p ⁵ 4d ³ (⁴ F) ⁵ D + 5 4p ⁵ 4d ³ (⁴ P) ⁵ D
312368.08	312698	-330	2	17 4d5f ³ F + 15 4p ⁵ 4d ³ (⁴ P) ⁵ P + 14 4d5f ³ P
313207.16	313434	-227	2	39 4d5f ³ F + 25 4d5f ¹ D + 9 4p ⁵ 4d ³ (² D) ³ F
313772.78	314068	-295	3	36 4d5f ³ F + 16 4p ⁵ 4d ³ (² F) ³ F + 10 4p ⁵ 4d ³ (² D) ³ F
313919.45	313743	176	4	61 4d5f ³ F + 7 4p ⁵ 4d ³ (² F) ³ F + 5 4p ⁵ 4d ³ (⁴ F) ⁵ D
314526.51	314494	33	4	52 4d5f ³ H + 15 4d5f ³ G + 12 4p ⁵ 4d ³ (² G) ³ G
315617.49	315048	569	5	55 4p ⁵ 4d ³ (² H) ³ I + 22 4p ⁵ 4d ³ (² H) ³ H + 8 4p ⁵ 4d ³ (² G) ³ H
315691.14	315526	165	3	24 4d5f ¹ F + 21 4d5f ³ F + 15 4d5f ³ G
316289.19	316628	-339	4	46 4d5f ¹ G + 10 4p ⁵ 4d ³ (² G) ¹ G + 8 4p ⁵ 4d ³ (² H) ³ H
316463.94	316224	240	5	79 4d5f ³ H + 8 4p ⁵ 4d ³ (² H) ³ I
316539.85	316044	496	1	39 4d5f ³ P + 24 4p ⁵ 4d ³ (⁴ P) ⁵ P + 10 4p ⁵ 4d ³ (² P) ³ S
316643.63	316831	-187	6	74 4d5f ³ H + 12 4p ⁵ 4d ³ (² H) ³ H + 8 4p ⁵ 4d ³ (² H) ¹ I
316690.26	316404	286	2	39 4d5f ³ P + 9 4p ⁵ 4d ³ (⁴ P) ⁵ P + 9 4p ⁵ 4d ³ (⁴ P) ⁵ D
319064.90	319214	-149	3	31 4p ⁵ 4d ³ (⁴ F) ⁵ D + 29 4p ⁵ 4d ³ (⁴ P) ⁵ D + 10 4p ⁵ 4d ³ (⁴ P) ⁵ P
319484.00	319614	-130	0	49 4p ⁵ 4d ³ (⁴ P) ⁵ D + 17 4p ⁵ 4d ³ (⁴ F) ⁵ D + 13 4p ⁵ 4d ³ (² P) ¹ S
319648.03	319104	544	5	48 4d5f ¹ H + 18 4p ⁵ 4d ³ (² G) ³ H + 8 4p ⁵ 4d ³ (² F) ³ G
319779.02	320146	-367	2	20 4p ⁵ 4d ³ (⁴ P) ⁵ P + 17 4p ⁵ 4d ³ (⁴ P) ³ D + 16 4p ⁵ 4d ³ (⁴ P) ⁵ D
320795.31	320432	363	3	28 4p ⁵ 4d ³ (⁴ F) ⁵ G + 12 4p ⁵ 4d ³ (² G) ³ G + 11 4d5f ¹ F
321070.92	320838	233	4	41 4p ⁵ 4d ³ (² G) ³ H + 12 4p ⁵ 4d ³ (⁴ F) ³ G + 8 4d5f ³ H
323010.78	323038	-27	3	41 4d5f ³ D + 18 4p ⁵ 4d ³ (² P) ³ D + 7 4d5f ¹ F

Table 7. continued.

E_{exp}^a	E_{calc}^b	ΔE	J	Leading components (in %) in LS coupling ^c
323076.60	323184	-107	1	17 4p ⁵ 4d ³ (⁴ P) ³ D + 14 4d5f ¹ P + 14 4d5f ³ D
323151.83	322790	362	4	22 4p ⁵ 4d ³ (² D) ³ F + 16 4p ⁵ 4d ³ (² F) ³ G + 14 4p ⁵ 4d ³ (⁴ F) ³ G
325021.00	326124	-1103	3	18 4p ⁵ 4d ³ (² D) ³ F + 15 4p ⁵ 4d ³ (² D) ¹ F + 14 4p ⁵ 4d ³ (² F) ³ F
325451.40	325785	-334	2	24 4p ⁵ 4d ³ (⁴ P) ⁵ P + 19 4d5f ³ D + 8 4p ⁵ 4d ³ (⁴ P) ⁵ D
325482.90	325966	-483	4	30 4p ⁵ 4d ³ (² D) ³ F + 20 4p ⁵ 4d ³ (⁴ F) ³ G + 10 4p ⁵ 4d ³ (² F) ³ F
325636.30	325093	543	5	36 4p ⁵ 4d ³ (⁴ F) ³ G + 27 4p ⁵ 4d ³ (² F) ³ G + 11 4p ⁵ 4d ³ (² H) ³ H
327058.60	327568	-509	2	17 4p ⁵ 4d ³ (⁴ P) ³ P + 10 4p ⁵ 4d ³ (² D) ³ P + 9 4p ⁵ 4d ³ (² F) ¹ D
327147.00	327349	-202	0	24 4p ⁵ 4d ³ (⁴ P) ³ P + 23 4d5f ³ P
329436.00	329202	234	2	12 4p ⁵ 4d ³ (⁴ P) ⁵ P + 12 4p ⁵ 4d ³ (² F) ³ F + 11 4p ⁵ 4d ³ (² P) ³ D
329481.50	329232	250	4	62 4p ⁵ 4d ³ (² H) ³ H + 10 4p ⁵ 4d ³ (² G) ¹ G + 9 4p ⁵ 4d ³ (⁴ F) ³ G
329793.78	330022	228	5	18 4p ⁵ 4d ³ (⁴ F) ³ G + 12 4p ⁵ 4d ³ (² G) ³ G + 12 4p ⁵ 4d ³ (² H) ³ H
330042.70	330219	-176	3	25 4p ⁵ 4d ³ (⁴ P) ³ D + 15 4p ⁵ 4d ³ (² F) ³ D + 10 4p ⁵ 4d ³ (² D) ³ F
331039.00	330940	99	5	45 4p ⁵ 4d ³ (² H) ³ H + 12 4p ⁵ 4d ³ (² F) ³ G + 9 4p ⁵ 4d ³ (² H) ³ I
331241.30	331773	-532	1	48 4p ⁵ 4d ³ (² P) ³ D + 16 4d5f ³ D + 7 4p ⁵ 4d ³ (² D) ³ D
333683.90	333950	-266	4	24 4p ⁵ 4d ³ (² G) ³ G + 23 4p ⁵ 4d ³ (² F) ¹ G + 20 4p ⁵ 4d ³ (² F) ³ G
335185.90	335792	-605	3	18 4p ⁵ 4d ³ (² D) ³ F + 12 4p ⁵ 4d ³ (² F) ³ G + 12 4p ⁵ 4d ³ (² D) ¹ F
335518.50	335117	402	0	45 4p ⁵ 4d ³ (² P) ³ P + 37 4p ⁵ 4d ³ (² D) ³ P + 13 4p ⁵ 4d ³ (² P) ¹ S
339075.10	338926	149	2	24 4p ⁵ 4d ³ (² D) ³ F + 15 4p ⁵ 4d ³ (² D) ³ P + 11 4p ⁵ 4d ³ (² P) ¹ D
339315.90	340261	-945	3	31 4p ⁵ 4d ³ (² F) ³ G + 17 4p ⁵ 4d ³ (² G) ³ G + 10 4d5f ³ G
339672.90	339529	144	5	39 4p ⁵ 4d ³ (² G) ¹ H + 20 4p ⁵ 4d ³ (² G) ³ G + 9 4p ⁵ 4d ³ (² G) ³ H
341107.60	341139	-31	2	44 4p ⁵ 4d ³ (² D) ³ P + 15 4p ⁵ 4d ³ (² P) ³ P + 13 4p ⁵ 4d ³ (² P) ¹ D
343064.20	343404	-340	4	29 4p ⁵ 4d ³ (² F) ¹ G + 16 4p ⁵ 4d ³ (² D) ³ F + 12 4p ⁵ 4d ³ (² F) ³ G
345339.60	346017	-677	3	28 4d6f ³ G + 16 4p ⁵ 4d ³ (² H) ³ G + 7 4d5f ³ G
347173.53	347194	-20	2	91 5s4f ³ F + 5 4p ⁵ 4d ² 5s(¹ G) ³ F
347303.47	347354	-51	3	90 5s4f ³ F
347509.30	347154	355	4	27 4d6f ³ G + 11 4p ⁵ 4d ³ (² H) ³ G + 5 4p ⁵ 4d ³ (² D) ³ F
347675.00	347626	49	4	84 5s4f ³ F
349517.60	349398	120	5	46 4d6f ³ G + 14 4p ⁵ 4d ³ (² H) ³ G + 10 4p ⁵ 4d ³ (⁴ F) ³ G
349710.90	349517	194	3	20 4p ⁵ 4d ³ (² D) ³ F + 17 4p ⁵ 4d ³ (² F) ³ F + 11 4p ⁵ 4d ³ (² D) ³ F
349902.70	349664	239	4	14 4p ⁵ 4d ³ (² F) ³ F + 14 4p ⁵ 4d ³ (² F) ³ G + 14 4p ⁵ 4d ³ (² F) ¹ G
350465.80	350509	-43	2	54 4d6f ¹ D + 23 4d6f ³ F + 5 4p ⁵ 4d ³ (² D) ¹ D
351332.70	351241	92	2	20 4d6f ³ F + 15 4d6f ³ D + 5 4p ⁵ 4d ³ (² D) ³ F
351932.60	352021	-88	3	28 5s4f ¹ F + 25 4d6f ¹ F + 17 4d6f ³ D
353002.30	352410	592	1	50 4d6f ³ D + 21 4d6f ³ P + 6 4d6f ¹ P
353268.90	353248	21	3	39 5s4f ¹ F + 20 4d6f ³ F + 18 4d6f ³ D
353671.83	353284	388	2	31 4d6f ³ D + 23 4d6f ³ P + 13 4d6f ³ F
354169.92	353899	271	3	47 4d6f ³ F + 29 4d6f ³ D
354247.00	354112	135	4	46 4d6f ³ F + 37 4d6f ³ H
354542.54	354315	227	5	53 4d6f ³ H + 25 4d6f ¹ H + 8 4d6f ³ G
354582.30	354480	102	2	30 4d6f ³ F + 14 4d6f ³ P + 11 4p ⁵ 4d ³ (² F) ³ F
354959.83	354943	17	4	55 4d6f ¹ G + 24 4d6f ³ F + 14 4d6f ³ H
355095.60	354717	379	0	82 4d6f ³ P + 11 4p ⁵ 4d ³ (⁴ P) ³ P
356149.65	356068	82	3	54 4d6f ¹ F + 19 5s4f ¹ F + 6 4d6f ³ D
356387.52	355899	489	5	43 4d6f ³ H + 35 4d6f ¹ H + 14 4p ⁵ 4d ³ (² H) ¹ H
358278.19	358202	76	1	84 4d6f ¹ P
359499.00	359424	75	3	28 4p ⁵ 4d ³ (² D) ³ D + 21 4p ⁵ 4d ³ (² D) ¹ F + 16 4p ⁵ 4d ³ (² D) ³ D
363720.60	366218	-2497	3	43 4d6f ³ G + 22 4d7f ³ G + 12 4p ⁵ 4d ³ (² H) ³ G
365766.80	368161	-2394	4	37 4d6f ³ G + 30 4d7f ³ G + 13 4p ⁵ 4d ³ (² H) ³ G
366751.60	366516	236	2	43 4p ⁵ 4d ³ (² D) ³ D + 24 4p ⁵ 4d ³ (² D) ³ D + 15 4p ⁵ 4d ³ (² F) ³ D
366892.60	369103	-2210	5	24 4d6f ³ G + 22 4d7f ³ G + 9 4p ⁵ 4d ³ (² H) ³ G
367517.40	367806	-289	2	36 4p ⁵ 4d ³ (² D) ¹ D + 35 4p ⁵ 4d ³ (² D) ¹ D + 8 4p ⁵ 4d ³ (² D) ³ F
368492.20	367727	765	3	23 4p ⁵ 4d ³ (² F) ¹ F + 19 4p ⁵ 4d ³ (² D) ¹ F + 17 4p ⁵ 4d ³ (² D) ³ D
371078.10	371292	-214	1	40 4d7f ³ D + 13 4d6f ³ D + 10 4p ⁵ 4d ³ (² D) ³ D
371811.60	372022	-210	2	25 4d7f ¹ D + 22 4d7f ³ D + 16 4d7f ³ F
372444.90	373055	-610	5	38 4d7f ¹ H + 16 4p ⁵ 4d ³ (² H) ¹ H + 16 4d7f ³ G
373453.50	373046	408	3	40 4d7f ³ D + 22 4d7f ¹ F + 6 4d7f ³ F

Table 7. continued.

E_{exp}^a	E_{calc}^b	ΔE	J	Leading components (in %) in LS coupling ^c
375034.50	374431	604	2	50 4d7f ³ F + 13 4d7f ³ P + 7 4p ⁵ 4d ³ (⁴ F) ³ F
375165.80	374710	456	1	57 4d7f ³ P + 9 4p ⁵ 4d ³ (⁴ P) ³ P + 6 4d6f ³ P
375355.10	374621	734	3	67 4d7f ³ F + 9 4p ⁵ 4d ³ (⁴ F) ³ F + 6 4d7f ¹ F
377569.20	375812	1757	4	64 4d7f ³ H + 25 4d7f ³ F
377999.30	376923	1076	4	57 4d7f ¹ G + 21 4d7f ³ H + 14 4d7f ³ F
378160.50	377083	1077	5	95 4d7f ³ H
381105.40	381993	-888	3	64 4d7f ³ G + 11 4d8f ³ G + 7 4p ⁵ 4d ³ (² H) ³ G
382612.30	383691	-1079	4	60 4d7f ³ G + 16 4d8f ³ G + 8 4p ⁵ 4d ³ (² H) ³ G
383279.50	384509	-1230	5	38 4d7f ³ G + 17 4d7f ¹ H + 12 4d8f ³ G
383895.40	383758	137	1	41 4d7f ³ D + 13 4d8f ³ D + 6 4p ⁵ 4d ³ (² F) ³ D
384886.50	385093	-206	3	67 4p ⁵ 4d ² 5s(³ F) ⁵ D + 23 4p ⁵ 4d ² 5s(³ P) ⁵ D + 5 4p ⁵ 4d ² 5s(³ F) ⁵ F
385431.20	385190	241	2	28 4d7f ³ D + 19 4d8f ³ D + 7 4p ⁵ 4d ³ (² F) ³ D
385599.50	387275	-1675	5	28 4d8f ¹ H + 20 4d7f ¹ H + 10 4p ⁵ 4d ³ (² H) ¹ H
386020.80	386175	-154	2	17 4d8f ¹ D + 15 4d8f ³ F + 9 4p ⁵ 4d ³ (⁴ F) ³ F
386919.80	387815	-895	1	36 4d8f ³ P + 21 4d7f ³ P + 10 4p ⁵ 4d ³ (⁴ P) ³ P
387095.30	387690	-595	2	19 4d8f ³ P + 17 4d8f ³ F + 10 4p ⁵ 4d ³ (⁴ F) ³ F
388410.00	387869	541	3	39 4d8f ³ F + 17 4p ⁵ 4d ³ (⁴ F) ³ F + 15 4d7f ³ F
389382.80	389203	180	4	52 4d8f ³ F + 12 4d8f ¹ G + 11 4p ⁵ 4d ³ (⁴ F) ³ F
389461.40	389065	396	3	37 4d8f ¹ F + 9 4d7f ¹ F + 8 4d8f ³ D
389545.00	389724	-179	2	33 4d8f ³ P + 22 4d8f ¹ D + 6 4d7f ¹ D
392544.30	391525	1019	4	56 4d8f ¹ G + 27 4d8f ³ H
393980.20	394029	-49	3	67 4d8f ³ G
394631.20	394261	370	1	45 4p ⁵ 4d ² 5s(³ F) ³ D + 21 4d8f ³ D + 7 4p ⁵ 4d ² 5s(³ P) ³ D
395094.50	394590	504	3	37 4d8f ³ D + 16 4p ⁵ 4d ³ (⁴ P) ³ D + 9 4p ⁵ 4d ³ (⁴ F) ³ D
395126.40	395145	-19	2	30 4p ⁵ 4d ² 5s(³ F) ³ D + 29 4d8f ³ F
396426.70	396630	-206	5	53 4d8f ³ G + 15 4d8f ¹ H + 7 4d9f ³ G
397682.60	397103	580	3	27 4d8f ³ F + 27 4p ⁵ 4d ² 5s(³ P) ⁵ P + 9 4p ⁵ 4d ³ (⁴ F) ³ F
398182.60	397729	454	2	20 4d8f ¹ D + 11 4d8f ³ P
401055.80	401385	-329	1	47 4d9f ³ D + 18 4p ⁵ 4d ³ (⁴ F) ³ D + 14 4d9f ¹ P
401751.20	401834	-83	4	46 4d9f ³ H + 45 4d9f ¹ G
401997.40	401396	601	2	46 4d9f ³ D + 17 4p ⁵ 4d ³ (⁴ F) ³ D + 7 4d9f ³ F

(a) From Reader & Tauheed (2015).

(b) This work.

(c) Only the first three components that are larger than 5% are given.

Table 8. Comparison between available experimental and calculated energy levels in Mo vi. Energies are given in cm⁻¹.

E_{exp}^a	E_{calc}^b	ΔE	J	Leading components (in %) in LS coupling ^c
Even parity				
0.00	0	0	1.5	99 4d ² D
2583.50	2583	0	2.5	99 4d ² D
119725.62	119725	0	0.5	99 5s ² S
282825.59	282825	0	1.5	99 5d ² D
283610.94	283611	0	2.5	99 5d ² D
313806.81	313807	0	0.5	100 6s ² S
386165.59	386166	0	1.5	99 6d ² D
386552.16	386552	0	2.5	99 6d ² D
395181.34	395181	0	3.5	100 5g ² G
395184.31	395184	0	4.5	100 5g ² G
400761.59	400762	0	0.5	100 7s ² S
439465.16	439465	0	1.5	99 7d ² D
439691.28	439691	0	2.5	99 7d ² D
443937.56	443938	0	3.5	100 6g ² G
443941.00	443941	0	4.5	100 6g ² G
447730.19	447730	0	0.5	100 8s ² S
470813.00	470813	0	1.5	99 8d ² D
470962.00	470962	0	2.5	99 8d ² D
473433.70	473434	0	3.5	100 7g ² G
473437.06	473437	0	4.5	100 7g ² G
474431.80	474432	0	5.5	100 7i ² I
474435.50	474436	0	6.5	100 7i ² I
492596.81	492597	0	3.5	100 8g ² G
492601.06	492601	0	4.5	100 8g ² G
493347.38	493347	0	5.5	100 8i ² I
493348.19	493348	0	6.5	100 8i ² I
Odd parity				
182404.47	182404	0	0.5	99 5p ² P
187331.19	187331	0	1.5	99 5p ² P
267047.22	266941	106	2.5	86 4f ² F + 11 4p ⁵ 4d ² (¹ G) ² F
267456.84	267566	-109	3.5	87 4f ² F + 8 4p ⁵ 4d ² (¹ G) ² F
286236.00	286288	-52	0.5	85 4p ⁵ 4d ² (³ F) ⁴ D + 13 4p ⁵ 4d ² (³ P) ⁴ D
287250.00	287263	-13	1.5	78 4p ⁵ 4d ² (³ F) ⁴ D + 16 4p ⁵ 4d ² (³ P) ⁴ D
288938.00	288902	36	2.5	67 4p ⁵ 4d ² (³ F) ⁴ D + 22 4p ⁵ 4d ² (³ P) ⁴ D + 6 4p ⁵ 4d ² (³ F) ⁴ F
300690.00	300600	90	2.5	87 4p ⁵ 4d ² (³ P) ⁴ P
303186.00	303246	-60	2.5	21 4p ⁵ 4d ² (³ F) ⁴ F + 38 4p ⁵ 4d ² (³ F) ⁴ G + 15 4p ⁵ 4d ² (³ F) ² F
304074.00	304043	31	1.5	82 4p ⁵ 4d ² (³ P) ⁴ P
306806.00	306871	-65	1.5	32 4p ⁵ 4d ² (¹ D) ² D + 36 4p ⁵ 4d ² (³ F) ⁴ F + 12 4p ⁵ 4d ² (³ F) ² D
307386.00	307433	-47	0.5	87 4p ⁵ 4d ² (³ P) ⁴ P + 5 4p ⁵ 4d ² (³ P) ² S
308874.00	308782	92	2.5	54 4p ⁵ 4d ² (¹ D) ² D + 15 4p ⁵ 4d ² (³ F) ² D + 9 4p ⁵ 4d ² (³ F) ⁴ G
312090.37	311918	172	3.5	39 4p ⁵ 4d ² (³ F) ⁴ F + 31 4p ⁵ 4d ² (³ F) ² G + 11 4p ⁵ 4d ² (³ F) ⁴ G
314953.00	314784	169	1.5	50 4p ⁵ 4d ² (³ F) ⁴ F + 20 4p ⁵ 4d ² (¹ D) ² P + 11 4p ⁵ 4d ² (¹ D) ² D
315155.49	315212	-57	2.5	21 4p ⁵ 4d ² (¹ G) ² F + 31 4p ⁵ 4d ² (³ F) ⁴ F + 17 4p ⁵ 4d ² (³ F) ² F
315795.00	316117	-322	0.5	68 4p ⁵ 4d ² (¹ D) ² P + 19 4p ⁵ 4d ² (³ P) ² P + 6 4p ⁵ 4d ² (³ P) ⁴ P
316476.56	316845	-368	3.5	25 4p ⁵ 4d ² (³ F) ² F + 25 4p ⁵ 4d ² (¹ G) ² F + 23 4p ⁵ 4d ² (³ P) ⁴ D
318528.00	318313	215	2.5	47 4p ⁵ 4d ² (³ P) ⁴ G + 28 4p ⁵ 4d ² (³ F) ⁴ F + 11 4p ⁵ 4d ² (¹ G) ² F
320088.00	319864	224	3.5	90 4p ⁵ 4d ² (¹ D) ² F + 5 4f ² F
329873.00	329987	-114	2.5	50 4p ⁵ 4d ² (³ P) ⁴ D + 26 4p ⁵ 4d ² (³ F) ⁴ D + 14 4p ⁵ 4d ² (³ P) ² D
331208.00	331187	21	3.5	41 4p ⁵ 4d ² (³ P) ⁴ D + 39 4p ⁵ 4d ² (³ F) ⁴ D + 8 4p ⁵ 4d ² (³ F) ⁴ F
331693.00	331458	235	1.5	47 4p ⁵ 4d ² (³ P) ⁴ D + 29 4p ⁵ 4d ² (³ P) ² D + 12 4p ⁵ 4d ² (³ F) ⁴ D
337018.00	336961	57	0.5	82 4p ⁵ 4d ² (³ P) ⁴ D + 12 4p ⁵ 4d ² (³ F) ⁴ D
337071.03	337150	-79	2.5	81 4p ⁵ 4d ² (¹ D) ² F
340570.78	340571	0	0.5	99 6p ² P
342562.44	342544	18	1.5	88 6p ² P + 5 4p ⁵ 4d ² (³ P) ² D

Table 8. continued.

E_{exp}^a	E_{calc}^b	ΔE	J	Leading components (in %) in LS coupling ^c
343114.50	343261	-146	1.5	45 4p ⁵ 4d ² (³ P) ² D + 24 4p ⁵ 4d ² (³ P) ⁴ D + 11 6p ² P
346888.80	346902	-13	1.5	77 4p ⁵ 4d ² (³ P) ⁴ S + 6 4p ⁵ 4d ² (³ P) ² D + 5 4p ⁵ 4d ² (³ P) ⁴ P
348702.28	348602	100	3.5	84 4p ⁵ 4d ² (¹ G) ² G + 9 4p ⁵ 4d ² (³ F) ² F
349283.97	349427	-143	2.5	65 4p ⁵ 4d ² (³ P) ² D + 14 4p ⁵ 4d ² (³ P) ⁴ D + 6 4p ⁵ 4d ² (³ F) ² D
355442.00	355442	0	1.5	69 4p ⁵ 4d ² (¹ S) ² P + 26 4p ⁵ 4d ² (¹ D) ² P
365103.41	365240	-137	2.5	51 5f ² F + 26 4p ⁵ 4d ² (³ F) ² F + 14 4p ⁵ 4d ² (¹ G) ² F
368203.16	368087	116	3.5	65 5f ² F + 16 4p ⁵ 4d ² (³ F) ² F + 11 4p ⁵ 4d ² (¹ G) ² F
394045.41	394049	-4	2.5	23 4p ⁵ 4d ² (³ F) ² F + 45 5f ² F + 21 4p ⁵ 4d ² (¹ G) ² F
398931.69	398943	-11	3.5	28 4p ⁵ 4d ² (¹ G) ² F + 33 5f ² F + 25 4p ⁵ 4d ² (³ F) ² F
403120.00	403201	-81	0.5	68 4p ⁵ 4d ² (³ P) ² P + 16 4p ⁵ 4d ² (¹ S) ² P + 11 4p ⁵ 4d ² (¹ D) ² P
407906.00	407574	332	1.5	71 4p ⁵ 4d ² (³ P) ² P + 16 4p ⁵ 4d ² (¹ D) ² P + 6 4p ⁵ 4d ² (¹ S) ² P
412799.00	412832	-33	2.5	68 4p ⁵ 4d ² (³ F) ² D + 15 4p ⁵ 4d ² (¹ D) ² D + 11 4p ⁵ 4d ² (³ P) ² D
413282.00	413433	-151	1.5	70 4p ⁵ 4d ² (³ F) ² D + 17 4p ⁵ 4d ² (¹ D) ² D + 9 4p ⁵ 4d ² (³ P) ² D
414853.81	414849	5	0.5	95 7p ² P
416068.59	416079	-10	1.5	95 7p ² P
417695.00	417842	-147	0.5	97 4p ⁵ 4d5s(³ P) ⁴ P
420665.00	420788	-123	1.5	93 4p ⁵ 4d5s(³ P) ⁴ P
426499.00	426529	-30	2.5	88 4p ⁵ 4d5s(³ P) ⁴ P + 8 4p ⁵ 4d5s(³ D) ⁴ D
427009.00	427117	-108	0.5	91 4p ⁵ 4d5s(³ P) ² P
431560.00	431267	293	3.5	87 4p ⁵ 4d5s(³ F) ⁴ F
433184.00	433248	-64	1.5	82 4p ⁵ 4d5s(³ P) ² P + 6 4p ⁵ 4d5s(³ D) ² D + 5 4p ⁵ 4d5s(³ D) ⁴ D
434125.00	433861	264	2.5	74 4p ⁵ 4d5s(³ F) ⁴ F + 8 4p ⁵ 4d5s(¹ F) ² F + 8 4p ⁵ 4d5s(³ F) ² F
436181.50	436073	109	2.5	93 6f ² F
436548.31	436660	-112	3.5	90 6f ² F
437890.00	437793	97	1.5	69 4p ⁵ 4d5s(³ F) ⁴ F + 19 4p ⁵ 4d5s(¹ D) ² D + 7 4p ⁵ 4d5s(³ D) ⁴ D
437978.00	437737	241	3.5	89 4p ⁵ 4d5s(³ F) ² F + 6 4p ⁵ 4d5s(³ D) ⁴ D
441562.00	441598	-36	2.5	54 4p ⁵ 4d5s(³ F) ² F + 22 4p ⁵ 4d5s(¹ D) ² D + 13 4p ⁵ 4d5s(³ D) ⁴ D
445102.50	445103	0	4.5	100 6h ² H
445106.20	445106	0	5.5	100 6h ² H
448052.00	448205	-153	3.5	68 4p ⁵ 4d5s(³ D) ⁴ D + 30 4p ⁵ 4d5s(¹ F) ² F
451836.00	451995	-159	2.5	38 4p ⁵ 4d5s(³ D) ² D + 32 4p ⁵ 4d5s(¹ F) ² F + 24 4p ⁵ 4d5s(³ D) ⁴ D
454862.00	454942	-80	0.5	72 4p ⁵ 4d5s(³ D) ⁴ D + 24 8p ² P
455807.00	455769	38	1.5	57 4p ⁵ 4d5s(³ D) ⁴ D + 18 4p ⁵ 4d5s(³ F) ⁴ F + 12 4p ⁵ 4d5s(¹ D) ² D
456494.90	456469	26	0.5	75 8p ² P + 22 4p ⁵ 4d5s(³ D) ⁴ D
456718.34	456722	-4	1.5	86 8p ² P + 7 4p ⁵ 4d5s(¹ D) ² D
458214.00	458360	-146	2.5	33 4p ⁵ 4d5s(¹ D) ² D + 19 4p ⁵ 4d5s(³ F) ² F + 18 4p ⁵ 4d5s(³ F) ⁴ F
458942.00	458974	-32	1.5	42 4p ⁵ 4d5s(¹ D) ² D + 24 4p ⁵ 4d5s(³ D) ² D + 19 4p ⁵ 4d5s(³ D) ⁴ D
462578.00	462592	-14	2.5	34 4p ⁵ 4d5s(³ D) ⁴ D + 39 4p ⁵ 4d5s(¹ D) ² D + 11 4p ⁵ 4d5s(³ D) ² D
466403.00	466383	20	1.5	65 4p ⁵ 4d5s(³ D) ² D + 17 4p ⁵ 4d5s(¹ D) ² D + 11 4p ⁵ 4d5s(³ P) ² P
466410.00	466382	28	3.5	61 4p ⁵ 4d5s(¹ F) ² F + 22 4p ⁵ 4d5s(³ D) ⁴ D + 11 4p ⁵ 4d5s(³ F) ⁴ F
467829.78	467813	16	2.5	98 7f ² F
467944.41	467961	-17	3.5	98 7f ² F
469446.00	469357	89	2.5	42 4p ⁵ 4d5s(¹ F) ² F + 39 4p ⁵ 4d5s(³ D) ² D + 14 4p ⁵ 4d5s(³ F) ² F
474295.97	474295	1	4.5	100 7h ² H
474296.78	474297	0	5.5	100 7h ² H
481343.00	481343	0	0.5	100 9p ² P
481768.00	481768	0	1.5	100 9p ² P
488713.00	488701	12	2.5	99 8f ² F
488752.00	488764	-12	3.5	99 8f ² F
493245.00	493246	-1	4.5	100 8h ² H
493248.34	493247	1	5.5	100 8h ² H
493377.60	493378	0	6.5	100 8k ² K
493381.30	493378	3	7.5	100 8k ² K
498038.00	498038	0	0.5	100 10p ² P
498300.00	498300	0	1.5	100 10p ² P
502976.00	502977	-1	2.5	100 9f ² F

Table 8. continued.

E_{exp}^a	E_{calc}^b	ΔE	J	Leading components (in %) in LS coupling ^c
503014.00	503013	1	3.5	100 9f 2F
509596.00	509596	0	0.5	100 11p 2P
509786.00	509786	0	1.5	100 11p 2P

(*a*) From Reader (2010).

(*b*) This work.

(*c*) Only the first three components that are larger than 5% are given.

Table 9. Comparison between available experimental and calculated energy levels in Mo vii. Energies are given in cm⁻¹.

E _{exp} ^a	E _{calc} ^b	ΔE	J	Leading components (in %) in LS coupling ^c
Even parity				
0.00	0	0	0	97 4p ⁶ 1S
542265.29	542456	-191	1	80 4p ⁵ 5p 3S + 17 4p ⁵ 5p 3P
544663.10	544655	8	1	73 4s4p ⁶ 4d 3D + 12 4p ⁴ (¹ D)4d ² 3D + 8 4p ⁵ 4f 3D
545906.83	545883	24	2	73 4s4p ⁶ 4d 3D + 11 4p ⁴ (¹ D)4d ² 3D + 8 4p ⁵ 4f 3D
548077.57	547987	91	2	55 4p ⁵ 5p 3D + 35 4p ⁵ 5p 1D + 8 4p ⁵ 5p 3P
548120.43	548120	0	3	74 4s4p ⁶ 4d 3D + 12 4p ⁴ (¹ D)4d ² 3D + 7 4p ⁵ 4f 3D
552329.97	552000	330	3	98 4p ⁵ 5p 3D
554401.01	554408	-7	1	48 4p ⁵ 5p 1P + 28 4p ⁵ 5p 3D + 18 4p ⁵ 5p 3P
557437.49	557605	-168	2	65 4p ⁵ 5p 3P + 29 4p ⁵ 5p 1D
563567.72	563589	-21	2	62 4s4p ⁶ 4d 1D + 18 4p ⁴ (¹ D)4d ² 1D + 9 4p ⁴ (¹ D)4d ² 1D
565803.85	565892	-88	0	77 4p ⁵ 5p 3P + 22 4p ⁵ 5p 1S
570658.75	570618	41	1	64 4p ⁵ 5p 3D + 33 4p ⁵ 5p 1P
577644.10	577596	48	2	34 4p ⁵ 5p 1D + 41 4p ⁵ 5p 3D + 23 4p ⁵ 5p 3P
577765.90	577851	-85	1	63 4p ⁵ 5p 3P + 18 4p ⁵ 5p 1P + 13 4p ⁵ 5p 3S
585026.11	585000	26	0	76 4p ⁵ 5p 1S + 23 4p ⁵ 5p 3P
609898.90	606995	2904	2	42 4p ⁴ (³ P)4d ² 5D + 22 4p ⁴ (³ P)4d ² 5F + 15 4p ⁴ (³ P)4d ² 5D
610564.98	610483	82	5	70 4p ⁵ 4f 3G + 24 4p ⁴ (³ P)4d ² 3G
610908.23	610998	-90	4	47 4p ⁵ 4f 3G + 22 4p ⁵ 4f 1G + 19 4p ⁴ (³ P)4d ² 3G
611395.80	614262	-2866	4	40 4p ⁴ (³ P)4d ² 5F + 29 4p ⁴ (³ P)4d ² 5D + 11 4p ⁴ (³ P)4d ² 5G
611727.25	611765	-38	1	54 4p ⁵ 4f 3D + 13 4p ⁴ (³ P)4d ² 5F + 10 4p ⁴ (³ P)4d ² 3D
613593.09	613685	-92	2	43 4p ⁵ 4f 3D + 8 4p ⁵ 4f 3F + 7 4p ⁴ (³ P)4d ² 3D
615203.92	615179	25	3	24 4p ⁵ 4f 3F + 24 4p ⁵ 4f 3G + 11 4p ⁴ (³ P)4d ² 3G
615725.35	615720	5	3	22 4p ⁴ (³ P)4d ² 5F + 17 4p ⁴ (³ P)4d ² 5D + 16 4p ⁵ 4f 3D
616148.25	616162	-14	4	38 4p ⁵ 4f 3F + 21 4p ⁴ (³ P)4d ² 3F + 20 4p ⁵ 4f 1G
624603.86	624455	149	2	26 4p ⁵ 4f 3F + 16 4p ⁵ 4f 1D + 12 4p ⁵ 4f 3D
633788.90	633559	230	3	24 4p ⁵ 4f 3G + 19 4p ⁵ 4f 3F + 18 4p ⁴ (³ P)4d ² 3G
635262.40	635075	187	4	32 4p ⁵ 4f 1G + 18 4p ⁴ (³ P)4d ² 3F + 11 4p ⁵ 4f 3G
635910.50	636296	-385	3	30 4p ⁵ 4f 1F + 19 4p ⁵ 4f 3D + 6 4p ⁴ (³ P)4d ² 3F
645811.86	645895	-83	2	26 4p ⁵ 4f 1D + 11 4p ⁴ (¹ D)4d ² 1D + 8 4p ⁵ 4f 3F
648282.60	647870	413	4	43 4p ⁴ (³ P)4d ² 5D + 24 4p ⁴ (³ P)4d ² 5D + 6 4p ⁴ (³ P)4d ² 3F
771708.20	770648	1060	1	15 4p ⁴ (³ P)4d ² 3P + 29 4p ⁵ 5f 3D + 11 4p ⁴ (¹ S)4d ² 3P
773033.30	769815	3218	2	56 4p ⁵ 5f 3D + 13 4p ⁵ 5f 3F + 8 4p ⁴ (³ P)4d ² 3D
774110.00	774662	-552	5	88 4p ⁵ 5f 3G + 7 4p ⁴ (³ P)4d ² 3G
775406.00	775927	-521	4	65 4p ⁵ 5f 3G + 12 4p ⁵ 5f 1G + 11 4p ⁵ 5f 3F
775781.00	774531	1250	3	45 4p ⁵ 5f 3D + 15 4p ⁵ 5f 3F + 15 4p ⁴ (³ P)4d ² 1F
776649.60	778934	-2284	2	20 4p ⁴ (¹ D)4d ² 3D + 21 4p ⁵ 5f 3D + 16 4p ⁴ (³ P)4d ² 3D
777161.10	777843	-682	3	33 4p ⁵ 5f 3G + 32 4p ⁵ 5f 1F + 22 4p ⁵ 5f 3F
779373.60	781310	-1936	4	48 4p ⁵ 5f 3F + 30 4p ⁵ 5f 1G
794751.20	794987	-236	2	59 4p ⁵ 5f 3F + 13 4p ⁵ 5f 1D + 13 4p ⁵ 5f 3D
797800.50	797278	522	3	43 4p ⁵ 5f 1F + 35 4p ⁵ 5f 3G + 13 4p ⁵ 5f 3D
797995.40	797598	397	3	45 4p ⁵ 5f 3F + 23 4p ⁵ 5f 3G + 18 4p ⁵ 5f 3D
800199.70	800881	-681	4	33 4p ⁵ 5f 1G + 25 4p ⁵ 5f 3G + 22 4p ⁵ 5f 3F
Odd parity				
302343.70	302618	-274	0	99 4p ⁵ 4d 3P
305558.90	305795	-236	1	96 4p ⁵ 4d 3P
312048.40	312226	-178	2	88 4p ⁵ 4d 3P + 9 4p ⁵ 4d 3D
315491.80	314944	548	4	99 4p ⁵ 4d 3F
318103.90	317625	479	3	83 4p ⁵ 4d 3F + 10 4p ⁵ 4d 1F + 6 4p ⁵ 4d 3D
322896.00	322759	137	2	66 4p ⁵ 4d 3F + 20 4p ⁵ 4d 1D + 13 4p ⁵ 4d 3D
333618.90	334040	-421	3	64 4p ⁵ 4d 3D + 35 4p ⁵ 4d 1F
341503.80	341537	-33	2	45 4p ⁵ 4d 1D + 33 4p ⁵ 4d 3F + 21 4p ⁵ 4d 3D
341713.00	341727	-14	1	95 4p ⁵ 4d 3D
347433.40	347624	-191	2	57 4p ⁵ 4d 3D + 31 4p ⁵ 4d 1D + 11 4p ⁵ 4d 3P
351126.60	350945	182	3	55 4p ⁵ 4d 1F + 29 4p ⁵ 4d 3D + 16 4p ⁵ 4d 3F

Table 9. continued.

E_{exp}^a	E_{calc}^b	ΔE	J	Leading components (in %) in LS coupling ^c
417528.60	417528	1	1	96 4p ⁵ 4d ¹ P
477767.80	477772	-4	2	99 4p ⁵ 5s ³ P
481295.99	481291	5	1	53 4p ⁵ 5s ¹ P + 45 4p ⁵ 5s ³ P
500618.75	500613	6	0	99 4p ⁵ 5s ³ P
502933.27	502939	-6	1	53 4p ⁵ 5s ³ P + 45 4p ⁵ 5s ¹ P
657602.91	657637	-34	0	99 4p ⁵ 5d ³ P
659015.62	659037	-21	1	88 4p ⁵ 5d ³ P + 9 4p ⁵ 5d ³ D
661488.47	661358	130	4	99 4p ⁵ 5d ³ F
661678.46	661689	-11	2	64 4p ⁵ 5d ³ P + 26 4p ⁵ 5d ³ D + 8 4p ⁵ 5d ¹ D
661683.19	661680	3	3	58 4p ⁵ 5d ³ F + 38 4p ⁵ 5d ¹ F
664362.66	664363	0	2	46 4p ⁵ 5d ¹ D + 31 4p ⁵ 5d ³ F + 21 4p ⁵ 5d ³ D
665713.78	665693	21	3	67 4p ⁵ 5d ³ D + 27 4p ⁵ 5d ¹ F
669063.09	669155	-92	1	46 4p ⁵ 5d ³ D + 50 4p ⁵ 5d ¹ P
684805.34	684824	-19	2	66 4p ⁵ 5d ³ F + 25 4p ⁵ 5d ¹ D + 7 4p ⁵ 5d ³ D
686113.49	686168	-55	2	45 4p ⁵ 5d ³ D + 32 4p ⁵ 5d ³ P + 20 4p ⁵ 5d ¹ D
686635.00	686656	-21	3	34 4p ⁵ 5d ¹ F + 37 4p ⁵ 5d ³ F + 29 4p ⁵ 5d ³ D
689784.69	689687	98	1	47 4p ⁵ 5d ¹ P + 43 4p ⁵ 5d ³ D + 8 4p ⁵ 5d ³ P
708843.60	708839	5	2	100 4p ⁵ 6s ³ P
710068.90	710073	-5	1	62 4p ⁵ 6s ¹ P + 37 4p ⁵ 6s ³ P
731864.90	731872	-7	0	99 4p ⁵ 6s ³ P
732582.50	732575	8	1	62 4p ⁵ 6s ³ P + 37 4p ⁵ 6s ¹ P
780390.00	780389	1	1	60 4s4p ⁶ 5p ³ P + 18 4p ⁴ (¹ D)4d5p ³ P + 13 4p ⁵ 6d ³ P
789696.00	789687	9	1	61 4s4p ⁶ 5p ¹ P + 20 4p ⁴ (¹ D)4d5p ¹ P + 8 4p ⁵ 6d ³ P
793700.50	793689	11	2	75 4p ⁵ 5g ³ F + 12 4p ⁵ 6d ³ D
793909.10	794182	-273	3	42 4p ⁵ 5g ³ F + 31 4p ⁵ 6d ³ D + 13 4p ⁵ 5g ¹ F
794550.20	794567	-17	6	99 4p ⁵ 5g ³ H
794669.80	794661	9	5	52 4p ⁵ 5g ¹ H + 47 4p ⁵ 5g ³ H
795532.00	795626	-94	1	54 4p ⁵ 6d ¹ P + 37 4p ⁵ 6d ³ D + 6 4s4p ⁶ 5p ¹ P
795665.20	795574	91	4	49 4p ⁵ 5g ³ F + 28 4p ⁵ 5g ³ G + 22 4p ⁵ 5g ¹ G
795918.60	795923	-4	3	39 4p ⁵ 5g ¹ F + 49 4p ⁵ 5g ³ G + 9 4p ⁵ 5g ³ F
796389.50	796411	-21	4	38 4p ⁵ 5g ¹ G + 31 4p ⁵ 5g ³ H + 30 4p ⁵ 5g ³ G
796442.60	796470	-27	5	68 4p ⁵ 5g ³ G + 16 4p ⁵ 5g ¹ H + 15 4p ⁵ 5g ³ H
816413.00	817148	-735	1	61 4p ⁵ 7s ¹ P + 33 4p ⁵ 7s ³ P
818278.10	818257	21	4	26 4p ⁵ 5g ³ G + 49 4p ⁵ 5g ³ F + 23 4p ⁵ 5g ¹ G
818504.10	818503	1	4	68 4p ⁵ 5g ³ H + 16 4p ⁵ 5g ¹ G + 15 4p ⁵ 5g ³ G
818583.40	818606	-23	3	48 4p ⁵ 5g ³ G + 30 4p ⁵ 5g ¹ F + 20 4p ⁵ 5g ³ F
818597.80	818598	0	5	37 4p ⁵ 5g ³ H + 31 4p ⁵ 5g ¹ H + 31 4p ⁵ 5g ³ G
839342.00	839304	38	1	65 4p ⁵ 7s ³ P + 35 4p ⁵ 7s ¹ P
874998.00	874906	92	1	43 4p ⁵ 8s ¹ P + 22 4p ⁵ 8s ³ P + 9 4p ⁴ (¹ D)4d5p ³ D
898093.00	897197	896	1	38 4p ⁵ 8s ³ P + 19 4p ⁵ 8s ¹ P + 6 4p ⁴ (³ P)4d5p ³ P
910830.00	910688	142	1	63 4p ⁵ 9s ¹ P + 33 4p ⁵ 9s ³ P
934536.00	934473	63	1	65 4p ⁵ 10s ¹ P + 33 4p ⁵ 10s ³ P

^(a) From Sugar & Musgrove (1988) and Shirai et al. (2000).^(b) This work.^(c) Only the first three components that are larger than 5% are given.

Table 10. Comparison of wavelengths and $\log gf$ values of the identified Mo v and Mo vi lines to literature values.

Ion	Transition	Energy / cm ⁻¹		$\lambda/\text{\AA}$	$\log gf$	$\lambda/\text{\AA}$	$\log gf$	
		Lower level	Upper level			this work		
Mo v	5p ³ P _{2,0} – 6s ⁵ S/2[5/2]3,0	157851	256676	1011.889	-0.12	1011.891	-0.16 ^a	
	5p ¹ D _{2,0} – 5d ³ F _{2,0}	146977	237760	1101.530	0.01	1101.529	0.07 ^a	
	5p ³ D _{1,0} – 5d ³ F _{2,0}	148949	237760	1125.988	0.22	1125.990	0.31 ^a	
	5p ³ F _{3,0} – 5d ³ F _{3,0}	151195	239069	1137.995	0.32	1137.999	0.39 ^a	
	5p ³ D _{3,0} – 5d ³ F _{4,0}	153040	240110	1148.502	0.45	1148.504	0.52 ^a	
	5p ³ F _{3,0} – 5d ³ G _{4,0}	151195	235496	1186.227	0.52	1186.230	0.57 ^a	
	5p ³ D _{1,0} – 5d ³ D _{1,0}	148949	233190	1187.061	0.03	1187.061	0.10 ^a	
	5s ³ D _{3,0} – 5p ³ P _{2,0}	94835	157851	1586.898	0.01	1586.890	0.09 ^a	
	5s ¹ D _{2,0} – 5p ¹ P _{1,0}	99380	162257	1590.414	-0.08	1590.415	0.01 ^a	
	5s ¹ D _{2,0} – 5p ¹ F _{3,0}	99380	159857	1653.541	0.28	1653.541	0.35 ^a	
	5s ³ D _{3,0} – 5p ³ F _{4,0}	94835	155032	1661.215	0.44	1661.215	0.51 ^a	
	5s ³ D _{2,0} – 5p ³ D _{3,0}	93111	153040	1668.662	0.15	1668.660	0.24 ^a	
	Mo vi	5p ² P _{1/2} – 5d ² D _{3/2}	182404	282826	995.806	0.35	995.811	0.44 ^b
	5p ² P _{3/2} – 5d ² D _{5/2}	187331	283611	1038.640	0.59	1038.642	0.67 ^b	
	5p ² P _{3/2} – 5d ² D _{3/2}	187331	282826	1047.182	-0.37	1047.184	-0.28 ^b	
	5d ² D _{5/2} – 5f ² F _{7/2}	283611	368203	1182.142	0.65	1182.143	0.72 ^b	
	5g ² G _{9/2} – 7h ² H _{11/2}	395184	474297	1264.023	0.31	1264.052	0.32 ^{b,c}	
	4d ² ² F _{7/2} – 5g ² G _{7/2}	316477	395184	1270.523	-1.04	1270.520	-0.91 ^b	
	4d ² ² F _{7/2} – 6d ² D _{5/2}	316477	386552	1427.030	-2.22	—	—	
	5s ² S _{1/2} – 5p ² P _{3/2}	119726	187331	1479.168	0.09	1479.168	0.15 ^b	
	5s ² S _{1/2} – 5p ² P _{1/2}	119726	182404	1595.435	-0.25	1595.435	-0.18 ^b	

Notes. ^(a) Reader & Tauheed (2015), ^(b) Reader (2010), Mo vi λ 1427.030 Å is not listed, ^(c) blend with 5g ²G_{7/2} – 7h ²H_{9/2}, λ 1264.017 Å, $\log gf = 0.23$.